VARIATIONS IN δ^{56}Fe DURING MAGMA DIFFERENTIATION AT CEDAR BUTTE VOLCANO: SIGNATURES OF THERMAL DIFFUSION?

BY

XIAOXIAO LI

THESIS

Submitted in partial fulfillment of the requirements
for the degree of Master of Science in Geology
in the Graduate College of the
University of Illinois at Urbana-Champaign, 2012

Urbana, Illinois

Adviser:

Professor Craig Lundstrom

Abstract

The Snake River Plain (SRP) is a volcanically active region lying along the Yellowstone hot spot track. Cedar Butte is a SRP volcanic complex which erupted a compositional progression of lavas from initial high silica rhyolite to final basaltic trachyandesite in the late pleistocene (~0.4 Ma). The lavas form a curved array on a MgO vs SiO_2 diagram, ruling out a primary role for mixing in producing this compositional sequence. This curvilinear variation is consistent with forward models of fractional crystallization from a tholeiitic basaltic parent (McCurry et al., 2008) implying that rhyolites and thus continental crust may form by extended fractionation from basalt.

To gain additional constraint on how magma differentiation from basalt to rhyolite might occur, I undertook an investigation of non-traditional stable isotope ratios in a suite of Cedar Butte lavas; I analyzed iron isotope ratios at UIUC by high resolution MC-ICPMS while the same samples were sent to University of Saskatchewan for Ca isotope analysis by thermal ionization mass spectrometry (TIMS). Analyzed Cedar Butte samples ranged from 58 wt% SiO_2 to 75 wt% SiO_2. Results show a smooth, upwardly curving progression of $\delta^{56}Fe_{IRMM-14}$ with increasing SiO_2. The most silicic samples have $\delta^{56}Fe$ of ~0.40 ‰ while the basaltic endmember has a $\delta^{56}Fe$ of ~0.10 ‰. $\delta^{44}Ca$ values show a less systematic but still analogous pattern as those of Fe isotopes.

This trend is unlikely to simply reflect fractional crystallization for two reasons: first, the predicted magnitude of fractionation of iron isotopes at inferred magmatic temperatures is smaller than observed. Second, the predicted sense of $\delta^{56}Fe$ fractionation occurring during magnetite removal is opposite to that observed; heavier isotopes should preferentially partition into magnetite based on theory. An alternative mechanism for producing the compositional

zoning and isotopic signature is a top down crystallization-reaction process involving a downward moving temperature gradient zone as suggested by Lundstrom (2009). Such a process differentiates the magma by a moving thermal migration zone while thermal diffusion isotopic fractionation leads to heavy isotope enrichment at the cold end of the gradient (in the most silicic material). Ultimately, the compositionally zoned mush is heated by arriving basaltic magmas leading to eruption.

Table of Contents

CHAPTER 1

INTRODUCTION

Earth has two major types of crust: an oceanic crust which is quite homogeneous and basaltic in composition and a continental crust which is much more heterogeneous and andesitic in bulk composition. The continental crust covers ~40% of the Earth's surface and the growth of continents remains an important scientific problem in geology (Taylor and White, 1965). In order to better understand the formation of the continental crust, we must identify the processes and mechanisms that produce the variety of rocks which constitute the crust.

The continental crust is heterogeneous with a general variation in composition with depth (Rudnick 1995). Although it is well accepted that the bulk composition of the upper crust is granodioritic (Taylor and McLennan, 1985), establishing the origin and the processes producing silicic (>65 wt% SiO_2 content) igneous rocks, and presumably the magmas forming them, remains a fundamental problem in igneous petrology. The genesis of high silica rhyolites, found in intraplate continental volcanic provinces, represents one of the biggest challenges and has been long debated (Bachmann and Bergantz 2004; McCurry et al. 2008).

It is generally considered that the combination of 1) partial melting of crustal material (e.g. Riley et al., 2001; Green and Fitz-Thomas, 1993); 2) fractional crystallization of a more mafic parent magma (e.g. Michael, 1983; Lindsay et al., 2001) contribute to the formation of silicic magmas. Numerous models have been invoked to explain the evolution of the magmas (e.g. crystal settling: Bowen, 1928; convective fractionation: Chen, & Turner, 1980; McBirney, 1985). Nevertheless, there remains a great deal of uncertainty about the actual process by which basaltic magmas differentiate into silicic ones; new ideas provide alternative mechanisms of differentiation. For instance, experiments examining water bearing partially molten andesite in a

temperature gradient show that a granitic mush forms at the cold end of the gradient (Huang et al., 2009). Notably, temperature gradients can also lead to large isotopic fractionations providing a possible signature of differentiation by this process.

Cedar Butte is a small volcano in the volcanically active eastern Snake River Plain (ESRP). The focus of this study is an eruptive sequence in the late Pleistocene (~0.4 Ma) that shows a compositional progression of lavas from initially erupted high silica rhyolite to final eruption of basaltic trachyandesite (McCurry et al., 2008). Because of their young age, excellent exposures, close spatial and temporal association with more mafic volcanic rocks and the highly distinctive geochemical characteristics of lower and upper crust and mantle in that area, these samples are perfect for examining and identifying the differentiation process leading to rhyolite magmas (McCurry et al. 2008).

Recently developed isotopic techniques provide a new tool to look into the magma differentiation process. For many years, it was concluded that most igneous rocks from the continental crust should not show significant fractionations of isotope ratios of heavy elements like Fe during differentiation. The basic reasoning is that equilibrium fractionation between phases should scale as $1/T^2$ such that at magmatic temperatures, the predicted fractionations are similar to or less than analytical precisions of <0.1 per mil (Beard et al., 2003; Poitrasson et al., 2004; Dauphas et al., 2004). However, it has now been repeatedly observed that significantly heavier δ^{57}Fe occurs in high-silica rocks (> 71%) indicating that some fractionation of Fe isotopes occurs during differentiation from mafic rocks to silicic rocks at high temperature (Poitrasson and Freydier, 2005). This observation has led to new speculations about the formation mechanism of rhyolite.

CHAPTER 2

GEOLOGICAL BACKGROUND AND SAMPLE SELECTION

The Eastern Snake River Plain is one of three sections of the Snake River Plain, which is divided into Western, Central and Eastern segments based on geophysical contrasts (Mabey, 1982). It overlaps the northern part of the late Cenozoic Basin and Range Province of the western U.S.A. (Kuntz, et al. 1980; Rodgers, et al. 1990). Most basalt of the ESPR volcanic field erupted from rift zones, including the closest rift to the study area the Arco rift zone (Cedar Butte is located near its southern terminus) and Great Rift (Hayden K P., 1992).

The ESRP is a well-know region of Pliocene to Quaternary olivine tholeiite volcanism. The stratigraphically and spatially associated volcanic deposits are referred as the Eastern Snake River Plain volcanic field (McCurry et al. 2008). The ESRP dominantly consists of an approximately 1 km thick layer of late Tertiary and Quaternary basaltic lavas and sedimentary rocks. However it also has compositionally distinctive evolved late stage Pleistocene intermediate to rhyolitic lavas, domes and tuffs in some areas (e.g. Leeman 1982b; Kuntz et al. 1986). These rocks stratigraphically overlie late Miocene to early Pliocene ignimbrite deposits and lava flows associated with the Yellowstone hotspot track (Rodgers, et al. 1990; Pierce and Morgan 1992). This study is limited to a younger, post-hotspot rock suite of the ESRP.

Cedar Butte is a shield volcano with a late-stage tephra cone exposed over an area of 35 km^2 and a relief of 218 meters, located in Bingham County, Idaho on the ESRP. It occurs near the southern termination of the Arco rift zone (ARZ), with Big Southern Butte (BSB) to the west and Middle Butte (MB) to the east (fig. 1d). Unlike most volcanic centers on the ESRP which are basaltic shields of olivine tholeiite, Cedar Butte lavas are more differentiated with compositions spanning from trachyandesite to potassic rhyolite (54 to 75% SiO_2) (Whitaker et al. 2008). Like

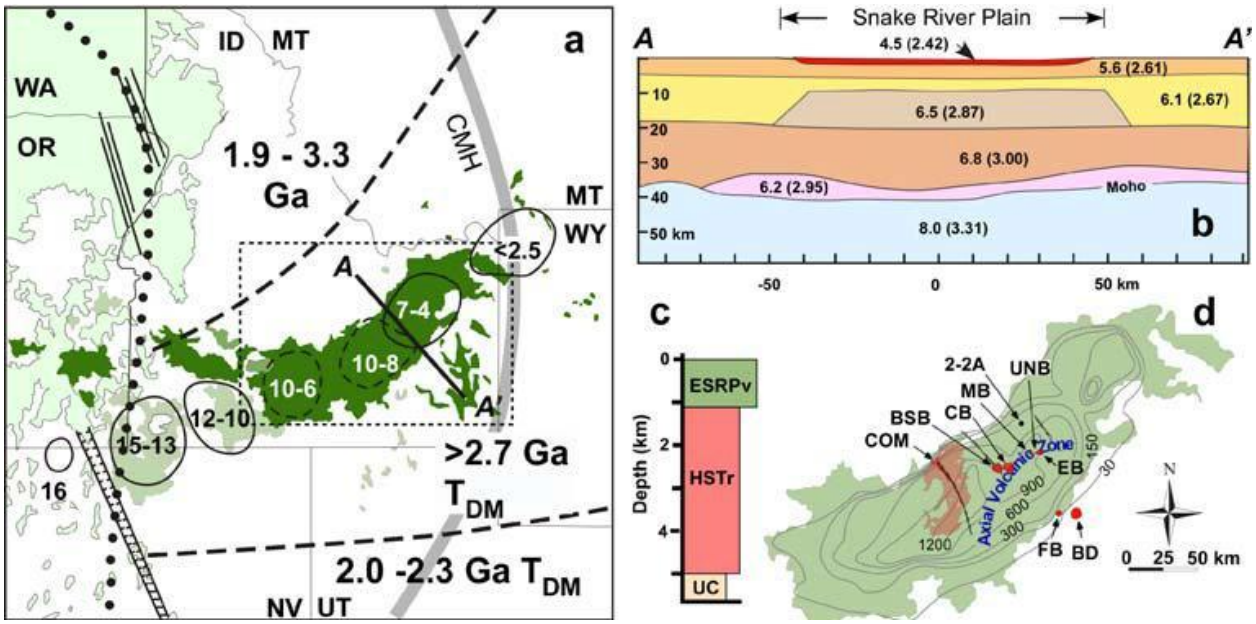

Figure 1 (by McCurry et al. 2008). **a** Geologic setting for the Eastern Snake River Plain and surroundings. Locations and ages (Ma) for silicic volcanic fields of the Yellowstone- Snake River Plain hotspot track are circled. A-A' is a cross section line for Fig. 1b. **b** Geophysical profile across the Eastern Snake River Plain illustrating mean seismic Vp velocities (km/s), densities (gm/cm^3), and layer thicknesses. **c** Simplified stratigraphy of the Eastern Snake River Plain. UC: pre-Tertiary upper crust; HSRr: Yellow stone-Snake River Plain hotspot track rhyolites; ESRPv: basalt-dominated rocks of the Eastern Snake River Plain volcanic field. **d** Expanded view of the Eastern Snake River Plain volcanic field.

most compositionally zoned eruption sequences which are thought to reflect zoning in the magma chamber prior to eruption, the eruption sequence of 0.4Ma goes from earliest erupted silicic rocks to latest erupted most mafic rocks. The rapid (< 100's years) sequential eruption produced mainly crystal-poor volcanic rocks with cumulative volumes of several ten's of km^3 (McCurry et al. 2008, Whitaker et al. 2008).

The rhyolites of Cedar Butte have all the classical characteristics of A-type granites, including high concentration of alkalies, high Fe/Mg and TiO_2/MgO ratios, as well as high concentrations of incompatible elements (Christiansen and McCurry, 2008).

Eight rock samples from Cedar Butte measured in this study include basaltic trachyandesite (CB-91-7), trachyandesite (CB-91-DI5), trachydacite (CB-91-48, CB-91-4, and CB-91-13), and rhyolite (CB-91-32, CB-91-DI1R, and CB-91-21) (Hayden K P., 1992). In addition, I analyzed one high silica rhyolite from nearby Big Southern Butte and one representative basalt sample from Craters of the Moon. These were added to the suite as they appear to form endmembers representative of parent basalt and final differentiate (McCurry, pers comm.).

The whole-rock major element concentrations are strongly correlated (Fig. 2a). Trends with silica vary from linear (e.g. FeO*) to curvilinear (e.g. MgO), including some with pronounced inflections (e.g. K_2O, Ba). Note that the curved array on MgO vs. SiO_2 eliminates a primary role of mixing. Trace element concentrations of the rock series also vary systematically with major element bulk composition, producing linear to strongly curvilinear to inflected co-variation trends (Whitaker et al. 2008).

The ε_{Nd} isotopic characteristics (ε_{Nd} = -4~-6) of ESPR rhyolites have an overlap with those of temporally related olivine tholeiites (e.g Craters of Moon). There is little evidence for contamination by lower Archaen crust which has a ε_{Nd} of -23~-47. The most evolved high-silica

rhyolites (~75-76% SiO_2) have slightly more evolved $^{87}Si/^{86}Sr_i$ (~0.7080 to 0.7097) compared to 0.706-0.708 for olivine tholeiites (Whitaker et al. 2008; Leeman, 1982a) but crustal contamination is still limited given the low Sr contents of the differentiated rhyolites in the ESRP.

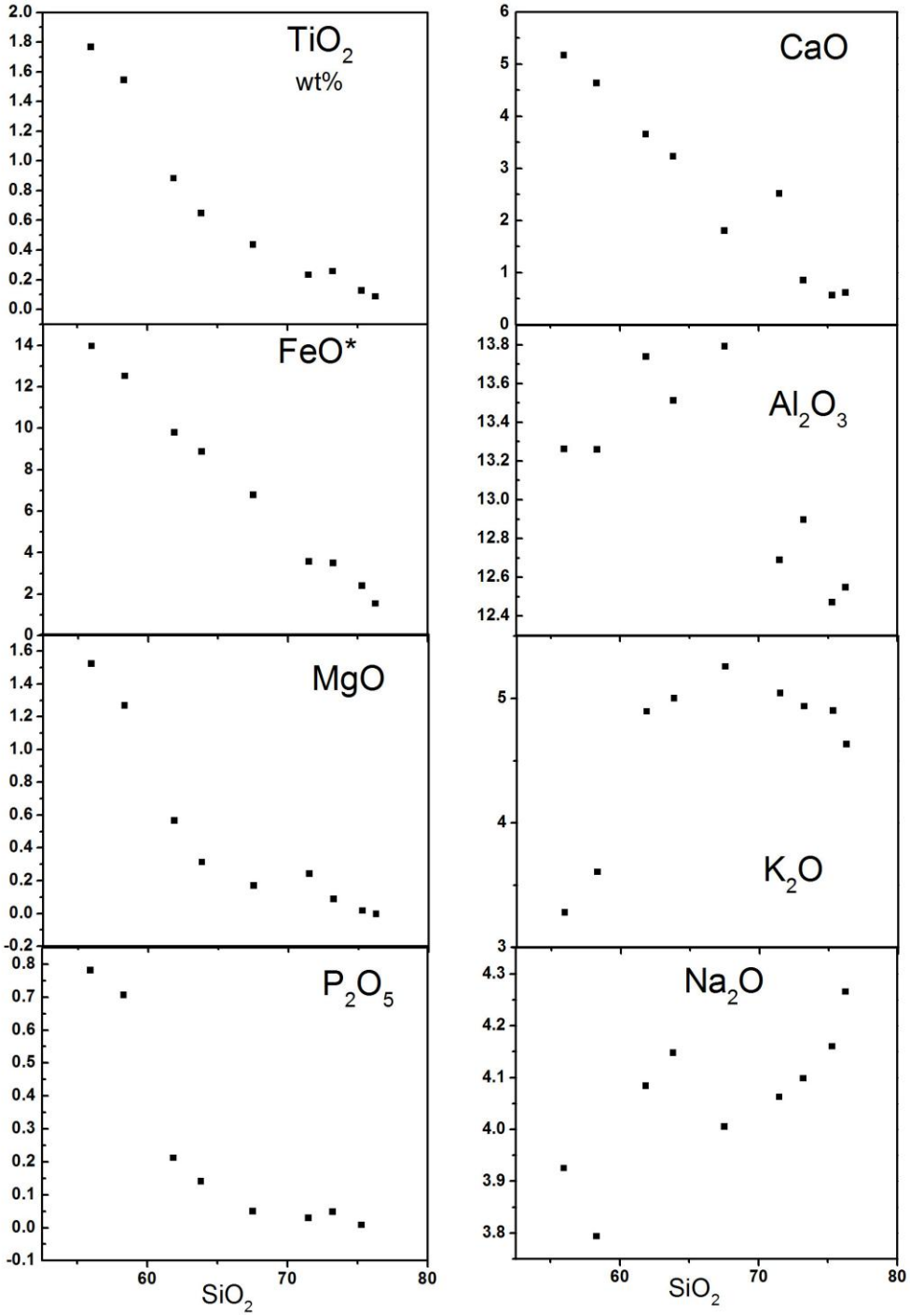

Figure 2 (a). Harker diagrams illustrating major-element variations versus SiO_2 content. All elements content are expressed in wt %. Data are from Michael McCurry and Karl P. Hayden, Idaho State University.

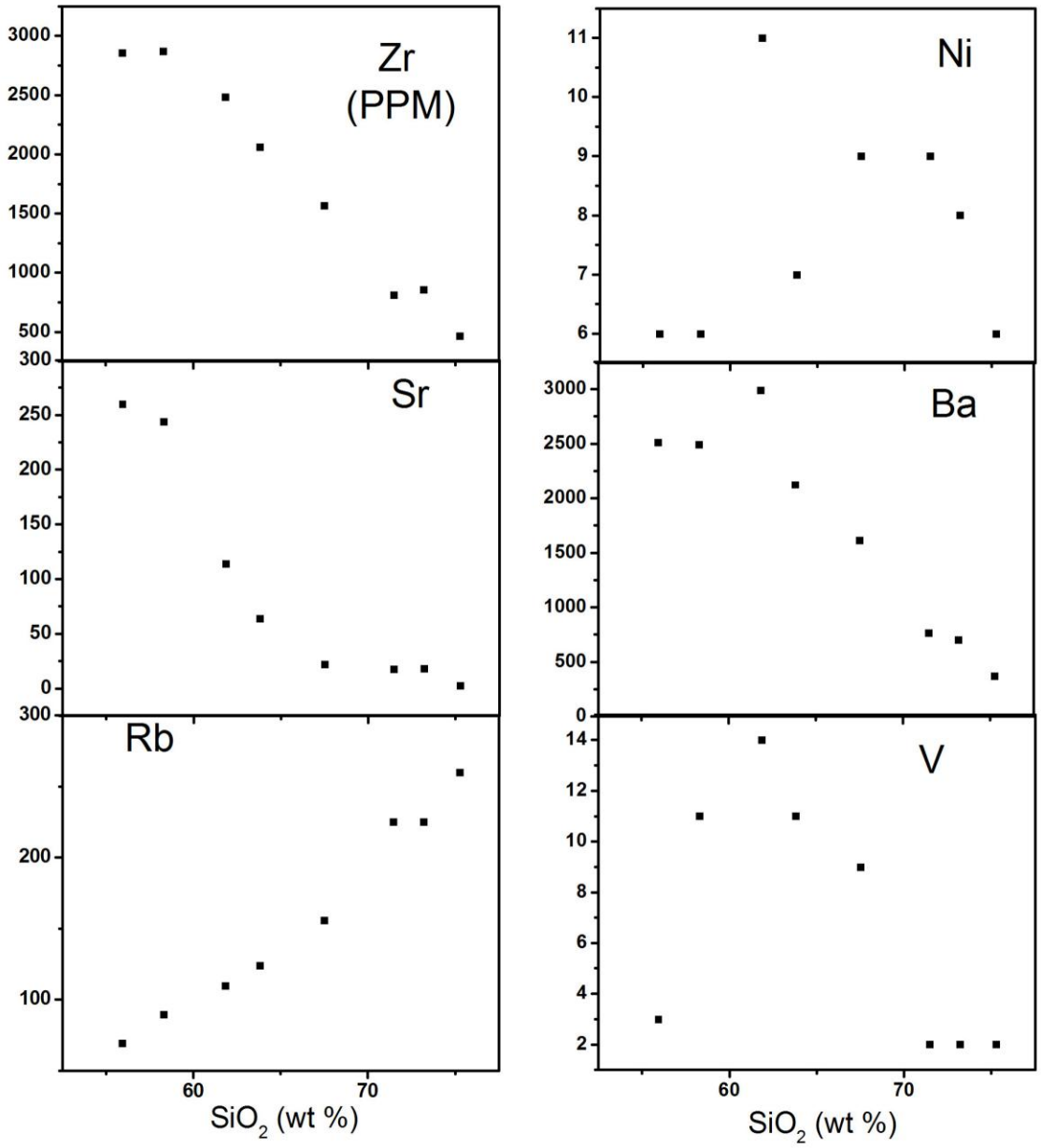

Figure 2 (b). Harker diagrams illustrating major-element variations versus SiO_2 content. Data are from Michael McCurry and Karl P. Hayden, Idaho State University.

CHAPTER 3

ANALYTICAL METHODS

While early attempts at measuring the stable isotopic composition of Fe used TIMS (Thermal ionization mass spectrometry) methods combined with a double spike technique, the variable instrumental mass fractionation led to inconvenience of measurement and poor precision (Dauphas N and Rouxel O, 2006). With the advent and development of MC-ICP-MS (multi-collector, inductively-coupled plasma mass spectrometry), these issues have been resolved with precisions of less than 0.1 per mil. Fe isotope studies by MC-ICP-MS are preferred because of the high ionization efficiency of Fe in the plasma and the rapid sample throughput possible with this instrument (Johnson C.M. et al, 2004). In this study, I have used MC-ICP-MS for high precision analyses following the methods described below.

1. Sample digestion

A few mg of whole rock powders were dissolved for multi-measurements. The samples were dissolved by adding a mixture of concentrated nitric and hydrofluoric acids in Teflon beakers (1:5). After being left capped on the hot plate for 2 days, the sample solutions were then dried down on a hot plate. The samples were dissolved again with concentrated nitric and hydrochloric acid to make sure dissolution was complete and then dried again on a hot plate. The samples were then dried down one more time using 8N hydrochloric acid, and eventually picked up in 0.4 ml 8N hydrochloric acid. The solution was put on a hotplate with cap overnight and was then ready for the separation process. These repeated evaporations were performed to get rid of insoluble fluorides and bring up any reduced Fe to fully oxidized Fe (III).

2. Chromatographic separation of iron

The isotopic analysis of Fe by MCICPMS is difficult due to the problems with isobaric ions that can potentially interfere with Fe isotope masses and matrix elements that can affect the mass bias on the mass spectrometer (Dauphas N and Rouxel O, 2006). As a result, before the isotopic analysis, Fe must be separated from the matrix elements such as Ca ($^{40}Ca^{16}O$ interference on ^{56}Fe), Mg and Cr (^{54}Cr on ^{54}Fe). The separation process is based on anion exchange chromatography in HCl medium on a strongly basic anion-exchange resin. Due to Fe (III)'s strong tendency towards chloride complex formation, the sorption of Fe (III) on anion exchange resin increases with HCl molarity. In contrast, Cr, Ca and several other elements are not quantitatively retained (Dauphas N and Rouxel O, 2006). Therefore Fe can stick to the column at high HCl molarity whereas other matrix and interfering elements are eluted with HCl. Fe is then subsequently eluted at lower molarity HCl (Strelow, 1980). In order to eliminate possible isotopic fractionation during the chemical separation process, 100% yield is required.

In my procedure, columns filled with 0.25 ml of AG1-X8 100-200 mesh anion exchange resin were previously cleaned with 8N HNO_3, H_2O and 0.1N HCl and then conditioned with 8N HCl. 0.2 ml of sample in 8N HCl solution was loaded on columns followed by 2 ml 8N HCl to elute the matrix elements from the column while Fe stayed fixed on the resin. The washout was collected for yield checks. Fe was then eluted from the column in sequence of 2 ml 0.5N HCl, 0.5 ml H_2O, 1 ml 8N HNO_3 and 0.5 ml H_2O. The solution was then dried down and taken up in 2% HNO_3 and was ready for isotopic analysis.

3. MC-ICP-MS analysis of Fe

The Iron isotope analysis was carried out on a double focusing Nu Plasma MC-ICP-MS in high resolution (HR) mode using the sample standard bracketing method at the Department of Geology in the University of Illinois at Urbana-Champaign.

3.1 Elimination of polyatomic mass interferences

Polyatomic interferences produced by the Ar plasma, including $^{40}Ar^{14}N$ on ^{54}Fe, $^{40}Ar^{16}O$ on ^{56}Fe, and $^{40}Ar^{16}OH$ on ^{57}Fe present major challenges for high precision Fe measurements by MC-ICP-MS. In order to minimize the relative intensities of argide and increase Fe ionization, a desolvating nebulizer was used. The large $^{56}Fe^{+}$ beam signal was measured on a 20V scale to prevent saturation of the amplifiers and increase the signal to baseline noise.

Along with using relatively high concentrations and thus signal sizes for Fe, the most important way to eliminate spectral interferences is high mass resolution through optical peak separation. To obtain high precision isotope measurements, it is essential to suppress mass interferences, and also to measure the isotopes on "flat top" peak shapes. This requires sufficiently small entrance slits to get an interference free space between the ion beams in the focal plane, and wide detector slits for the flat top peak to achieve their maximum width (Weyer and Schiwieters-spelling?, 2003). In the "pseudo high resolution" mode, the Fe^{+} peaks are resolved from argide interferences as flat topped shoulders on the low mass side of argide peaks (Dauphas et al., 2009). The mass resolution is expressed as the resolving power and defined as $m/ (m_{0.95}-m_{0.05})$ where m, $m_{0.95}$ and $m_{0.05}$ represent the masses measured at the peak, 5% and 95% intensity peak heights (Weyer and Schiwieters, 2003). The higher the resolving power, the steeper the peak slope and the broader the flat plateau region, which represents the interference-free space between the ion beams (Weyer and Schiwieters, 2003). The sensitivity for Fe is

reduced as the size of the entrance slit is reduced (as resolution gets higher). Therefore, the resolution has to be high enough to safely resolve polyatomic interferences from Fe isotopes while at the same time guaranteeing sufficient ion transmission efficiency.

3.2 Instrumental Mass Bias corrections

Another big challenge in the measurements is discriminating mass-dependent isotopic fractionation produced in the laboratory and instrument, from naturally occurring mass-dependent isotopic fractionation. Mass bias (the instrumental mass fractionation), is the variable transmission of the different isotope beams into the mass spectrometer (Albarede and Beard, 2004). For Fe isotopes the mass bias in MC-ICPMS can reach as high as 3.5% to 5.5% per amu (Dauphas N and Rouxel O, 2006). A variety of methods has been developed to make precise and accurate isotope measurements with a precision often better than 0.1‰ per amu. One of the most commonly used methods is the standard bracketing method in which measurement of an unknown sample is interpolated between two standard runs, one preceding and one following the sample analysis (Albarede and Beard, 2004). The isotopic composition of an unknown sample is then derived from the measurements of standards with known Fe isotope compositions.

3.3 The IRMM-014 standard

Stable isotope ratios are typically reported in "delta notation", δ, where the isotopic composition is normalized to a widely distributed, homogeneous, isotopic standard (Dauphas N and Rouxel O, 2006). In the case of Fe, the most commonly used standard is a pure Fe metal reference material IRMM-014 (Taylor et al., 1992), distributed by the Institute for Reference Materials and Measurements of the European Commission (Dauphas N and Rouxel O, 2006). As a result, all Fe isotopic ratios were reported relative to IRMM-014 in δ notation: $^{i}\delta Fe$ (‰) = $[(^{i}Fe/^{54}Fe)_{sample}/(^{i}Fe/^{54}Fe)_{IRMM\text{-}014}\text{-}1]\times 1000$ in this study.

During the analysis process, samples and standards were diluted to approximately 2 ppm in 2% double distilled HNO_3, yielding a signal of ~17 V on ^{56}Fe in the high resolution mode (mass resoling ~6000) The solutions were run using a Cetac ASX-110 auto-sampler and introduced to the Nu- Plasma via a desolvating nebulizer (DSN-100) with an uptake rate of 0.1ml/min. Each block of analysis consisted of 20 cycles of 8 second integrations with two separate rinses of 5% HNO_3 followed by two 2% HNO_3 rinses (4 minutes total rinse) in between sample and standard analyses to avoid cross-contamination. Each sample was usually repeatedly measured and bracketed by IRMM-014 four times, which takes approximately one hour. The isotope beams were measured using 3 Faraday cups: H4 for ^{56}Fe, H6 for ^{57}Fe and L3 for ^{54}Fe. 54Cr was measured on L5 and a correction for 54Cr was applied but usually negligible. The Na, Al, Mg, and Ca matrix cation contents within the purified Fe solutions were routinely checked and were found to have negligibly small concentrations.

4. Analysis methods for Ca isotope fractionation

Measurement of Ca isotope ratios is mainly done using thermal ionization mass spectrometry because plasma mass spectrometry analysis is degraded by the large 40Ar interference. The method of double spike is used to discriminate mass dependent fractionation in nature (up to ~ ±0.1% per mass unit) from mass dependent fractionation in the mass spectrometer (~ ±0.5% per mass unit for TIMS) (e.g. Russell et al. 1978; Skulan et al. 1997). The Ca isotope analyses in this study were performed in the Saskatchewan Isotope Laboratory (Department of Geological Sciences, University of Saskatchewan) by Chris Holmden with a ^{43}Ca-^{42}Ca double spike using a Thermo Finnigan Triton TIMS following methods described in Holmden and Belanger (2010). Calcium was purified from matrix elements using AG-MP50 cation exchange resin in gravity flow columns prior to mass spectrometry (Holmden et al. 2012).

The measured Ca isotope ratios are expressed as $\delta^{44}Ca$ values relative to seawater (Schmitt et al. 2003a, b). $\delta^{44}Ca$ (‰) = $[(^{44}Ca/^{40}Ca)_{sample}/ (^{44}Ca/^{40}Ca)_{seawater} -1] \times 1000$. Originally, aliquots of samples dissolved at UIUC were sent to Saskatchewan. Due to the very different value for sample CB91-32 and worry of incomplete dissolution (complication of having a CaF2 precipitate), the powder of this sample was sent to Holmden for a completely separate dissolution and analysis.

CHAPTER 4

ISOTOPIC RESULTS

Two MC-ICPMS instrumental sessions offset by an interval of one month, one in January, 2009 and one in February, 2009, were made in this study using two individual digestions of the same raw rock powder. Iron isotope results are reported in Table 3. The external precision was calculated from replicate measurements of the solution relative to IRMM-014.

1. Fe isotope ratios

1.1 Fe isotope ratios of igneous rock standards

The precision and accuracy can be evaluated by analyses of well- studied rock standards AGV-1 (Andesite standard from Guano Valley), BCR-1 and BCR-2 (basalt standard form the Columbia River) and NOD-P (manganese nodule from Pacific Ocean). The delta values of these standards measured in February are generally smaller than those measured in January, indicating a systemic bias in δ^{56}Fe between measurements in different days. This can be attributed to variations in the ability to correct for mass bias. Several standards made by bulk dissolution and making of a master solution for aliquoting (under "long-term storage") were measured also. The results showed relatively large difference between newly digested standards and those stored over long durations, which can be caused by isotopic fractionation happening in the storage container. Therefore, it is better to use freshly digested and diluted samples for running.

Generally, the results for δ^{56}Fe and δ^{57}Fe are consistent with mass dependent fractionation; however, the stronger signal on 56Fe usually means that precision and accuracy are better on the δ^{56}Fe measurement. Thus, I concentrate on reporting this value. The average δ^{56}Fe of AGV-1 is 0.144±0.144‰ (2SD, n=24), and δ^{57}Fe is 0.185±0.196‰. The δ^{56}Fe value is consistent with the

literature values reported by Beard et al. (2003) (0.130±0.102‰). For the BCR-1 standard, the weighted average δ^{56}Fe is 0.083±0.127‰ (2SD, n=24), consistent with previously reported results (Beard et al. (2003) Butler et al. (2005), Poitrasson et al. (2004) and Rouxel et al. (2003)). Thus, the isotope ratios of standards measured in this study are generally in good agreement with previous studies, indicating relatively accurate measurements were performed.

1.2 Fe isotope ratios of Cedar Butte rock samples

Eight rock samples from Cedar Butte and one sample from Big Southern Butte were measured for Fe isotopic ratios. Their FeO* contents vary from 2.4 (CB-91-21) to 14.0 wt. % (CB-91-7) and SiO_2 from 55.9 (CB-91-7) to 75.3 wt. % (CB-91-21) (Hayden K P., 1992) (Table 1). BSB-1 from Big Southern Butte is the most evolved sample with 1.6 wt. % for FeO* content and 76.3 wt. % for SiO_2 content (McCurry et al. 2008) (Table 1).

The average δ^{56}Fe of rocks from Cedar Butte, ranging in composition from basaltic trachyandesite to rhyolite, vary from 0.143±0.150‰ (2SD, n=24) to 0.436±0.103‰ (2SD, n=16). The three most mafic samples in this rock suite, CB-91-7, CB-91-DI5, and CB-91-48, have an average δ^{56}Fe value of 0.166±0.113‰ (2SD, n=16), 0.168±0.142‰ (2SD, n=27), and 0.143±0.150‰ (2SD, n=24) respectively, showing they are indistinguishable in δ^{56}Fe. Therefore no obvious variations in Fe isotopes were observed from the basaltic trachyandesites, trachyandesites and less evolved trachydacites with SiO_2 <62 wt. % of Cedar Butte (Fig. 3a). In the more silicic rocks, the δ^{56}Fe values have a trend of increasing from 0.223±0.182‰ (2SD, n=16) for the trachydacite sample CB-91-4 (SiO_2 = 63.8 wt. %) to 0.436±0.103‰ (2SD, n=16) for the rhyolite sample CB-91-21 (SiO_2 = 75.3 wt. %) (Fig. 3a). Analogous correlations exist between δ^{56}Fe and other major and trace element such as FeO (Fig. 3b) and MgO (Fig. 3c).

1.3 Comparisons with Fe isotopic compositions of terrestrial igneous rocks

Literature reported Fe isotopic ratios of terrestrial igneous rocks are list in Table 2 and plotted in Fig. 3a (Poitrassona and Freydier, 2005; Schoenberg and von Blanckenburg, 2006). An approximately 0.33‰ variation in $\delta^{56}Fe$ of terrestrial igneous samples is found, ranging from 0.055 ± 0.046 (2SD, Bergell intrusion with the smallest SiO_2 content 54.89 wt. %) to 0.386 ± 0.027 (2SE, Peralkaline granite, SiO_2 =76.8 wt. %). There is a slight systematic difference between the $\delta^{56}Fe$ values of Cedar Butte volcanic rocks and previously reported literature igneous rocks. The fact that Cedar Butte samples are systematically 0.1~0.2‰ heavier can be the consequence of instrumental bias and they are in the range of previously published terrestrial igneous rocks in consideration of uncertainties (Fig. 3a). These literature $\delta^{56}Fe$ values show an analogous pattern as those of Cedar Butte samples with indistinguishable variations in $\delta^{56}Fe$ within the less evolved SiO_2 range and continuously increase in $\delta^{56}Fe$ within the silicic series.

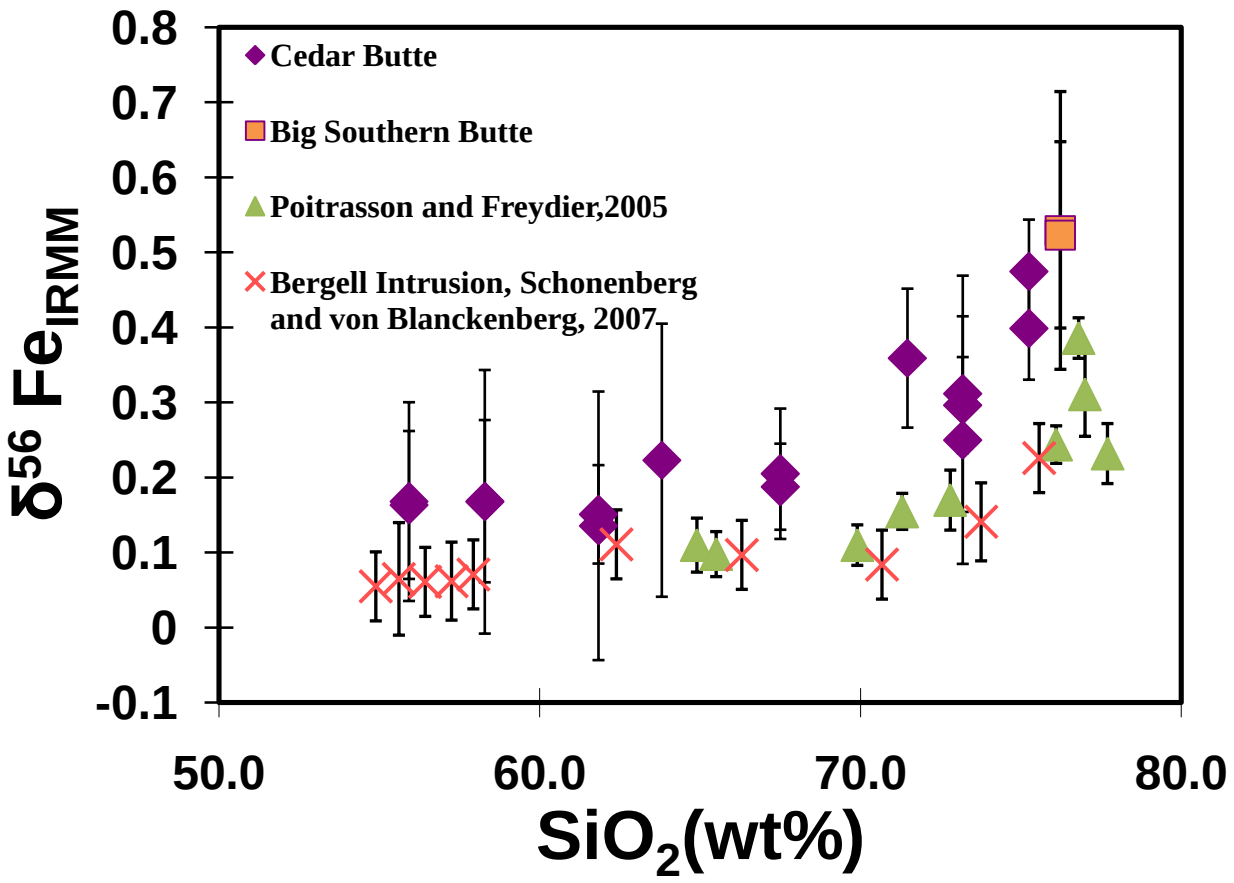

Fig. 3a. Iron isotope composition of Cedar Butte rocks as a function of SiO_2 content. Previously reported literature $\delta^{56}Fe$ values of terrestrial igneous rocks are shown for comparison (Poitrassona and Freydier, 2005; Schoenberg and von Blanckenburg, 2006).

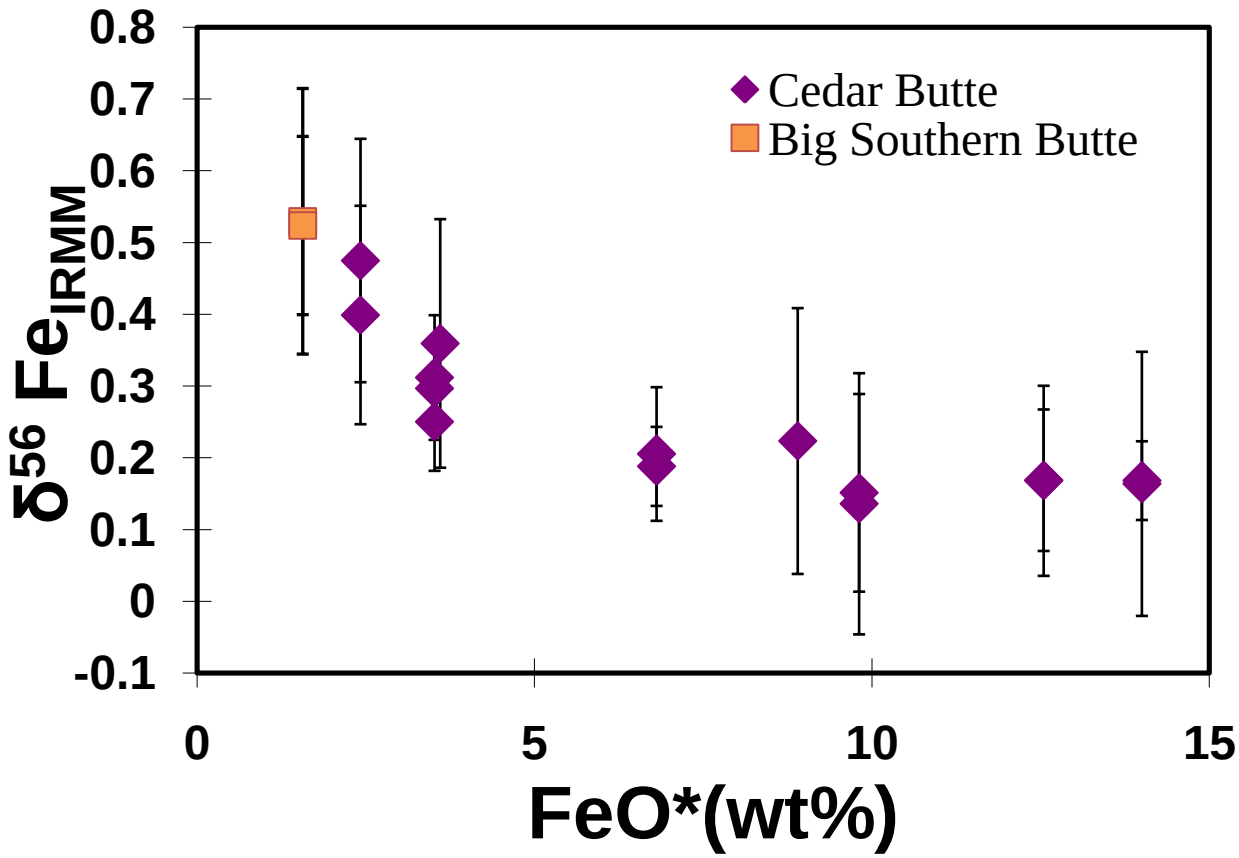

Fig. 3b. Iron isotope composition of Cedar Butte rocks as a function of FeO* (total iron) content.

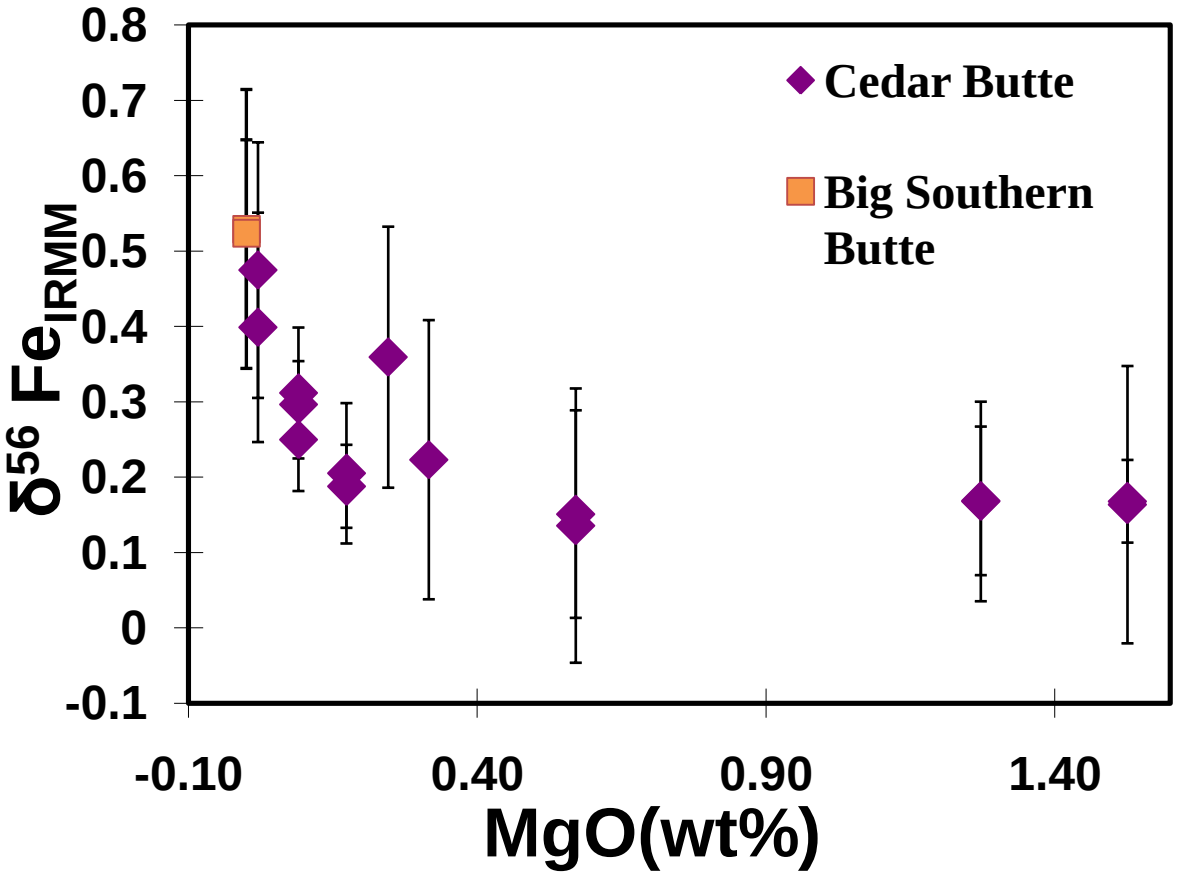

Fig. 3c. Iron isotope composition of Cedar Butte volcanic rocks as a function of MgO content. Error bars are 2 S. D. of all measured whole rocks. Each error bar correspond individual measurements. The δ^{56}Fe of high silica rhyolites become significantly heavier than intermediate volcanic rocks.

2 Ca isotope ratios

The same eight rock samples from Cedar Butte and one sample from Big Southern Butte were measured for Ca isotopic ratios. The CaO contents of these samples vary from 0.57 wt. % (CB-91-21) to 5.18 wt. % (CB-91-7) (McCurry et al. 2008) (Table 1).

2.1 Ca isotopic composition of Cedar Butte Samples

The measured δ^{44}Ca values of Cedar Butte samples range between -2.42 ± 0.12‰ (2SD, n=3) and -0.89 ± 0.04‰ (2SD, n=2) relative to seawater (Table 4). The sample from Big Southern Butte with the highest SiO_2 content among these rocks has the heaviest δ^{44}Ca value of -0.86 ± 0.03‰ (2SE). The four most mafic samples in this rock suite, CB-91-7, CB-91-DI5, CB-91-48, and CB-91-4 have an average δ^{44}Ca value of -1.09 ±0.03‰ (2SE), -1.10 ±0.03‰ (2SE), -1.32 ±0.27‰ (2SD, n=2), and -1.19 ±0.27‰ (2SD, n=2) respectively. There are no obvious variations in Ca isotopes in the basaltic trachyandesites, trachyandesites and less evolved trachydacites with SiO_2 <65 wt. % of Cedar Butte (Fig. 3). In the more silicic rocks, the δ^{44}Ca values have a trend toward increasingly heavy values from -1.08 ± 0.03‰ (2SE) for the trachydacite sample CB-91-13 (SiO_2 = 67.5 wt. %) to -0.89 ±0.04‰ (2SD, n=2) for the rhyolite sample CB-91-DI-1R (SiO_2 = 73.2 wt. %) and -0.86 ± 0.03‰ (2SE) for the Big Southern Butte rhyolite BSB (SiO_2 = 76.2 wt. %) (Fig. 4a).

Sample CB91-32 was measured three separate times including a separate dissolution and spiking in Prof. Holmden's lab. The highly unusual light isotopic signature of -2.3 appears to be real. Compared with previously measured igneous rocks (Fig. 4b), it stands out as being as much 1.5 per mil lighter than anything else.

2.2 Comparisons with Ca isotopic compositions of terrestrial volcanic rocks

Literature reported Ca isotopic ratios of terrestrial volcanic rocks are listed in Table 5 and plotted in Fig. 4b (Skulan et al. 1997; DePaolo 1994; Eiler et al. 1996 1997; Sims et al. 1999; Chen et al. 1999; Getty and DePaolo 1995; Richter et al. 2003). The standard used by early studies is ultrapure $CaCO_3$ (NIST 915a) and has a value of -0.92±0.18 (2SD) relative to the seawater standard used now (Skulan et al. 1997). Hence, 0.92 has been subtracted from literature $\delta^{44}Ca$ values to make them compatible with the seawater standard. An approximately 0.64‰ variation in $\delta^{44}Ca$ of terrestrial igneous samples is found, ranging from -1.19±0.12 (2SD, SUNY MORB), -1.19±0.06 (2SD, Shasta Dacite) to -0.58±0.25 (2SD, Mauna Kea Alkali basalt). This indicates small variations among volcanic rock samples. The Cedar Butte samples are in the range of previously reported terrestrial igneous rocks (Fig. 4b).

2.3 Anomalous Ca sample

There is an anomalous sample, CB-91-32 ($\delta^{44}Ca$=-2.42±0.12, 2SD; SiO_2 =71.5 wt. %), with an extremely light $\delta^{44}Ca$ composition which is ~1.5‰ lighter than the average Cedar Butte sample values (Fig. 4a). Replicate dissolutions and measurements were performed to make sure that no mistakes were involved in the analytical procedures. CaO contents of Cedar Butte samples decrease with increasing SiO_2 wt% and show a positive linear correlation with silica content (except sample CB-91-32; Fig. 2a), demonstrating that this sample has relatively higher CaO content as well. This suggests a possibility of mixing and assimilation with some high CaO content material. The weathering of Ca from silicates can give rise to isotope fractionation and produce isotopically lighter calcium carbonates. However the average carbonate rock is only ~0.5 lighter than the average igneous rocks (DePaolo, 2006), hence is not depleted enough to explain the 1.5 difference. Observations suggest that biological process could fractionate Ca

isotopes and lead to significantly lighter $\delta^{44}Ca$ as low as ~-4 (DePaolo, 2006). Without other evidences and constraints, the reason for this anomalously light sample will remain a mystery.

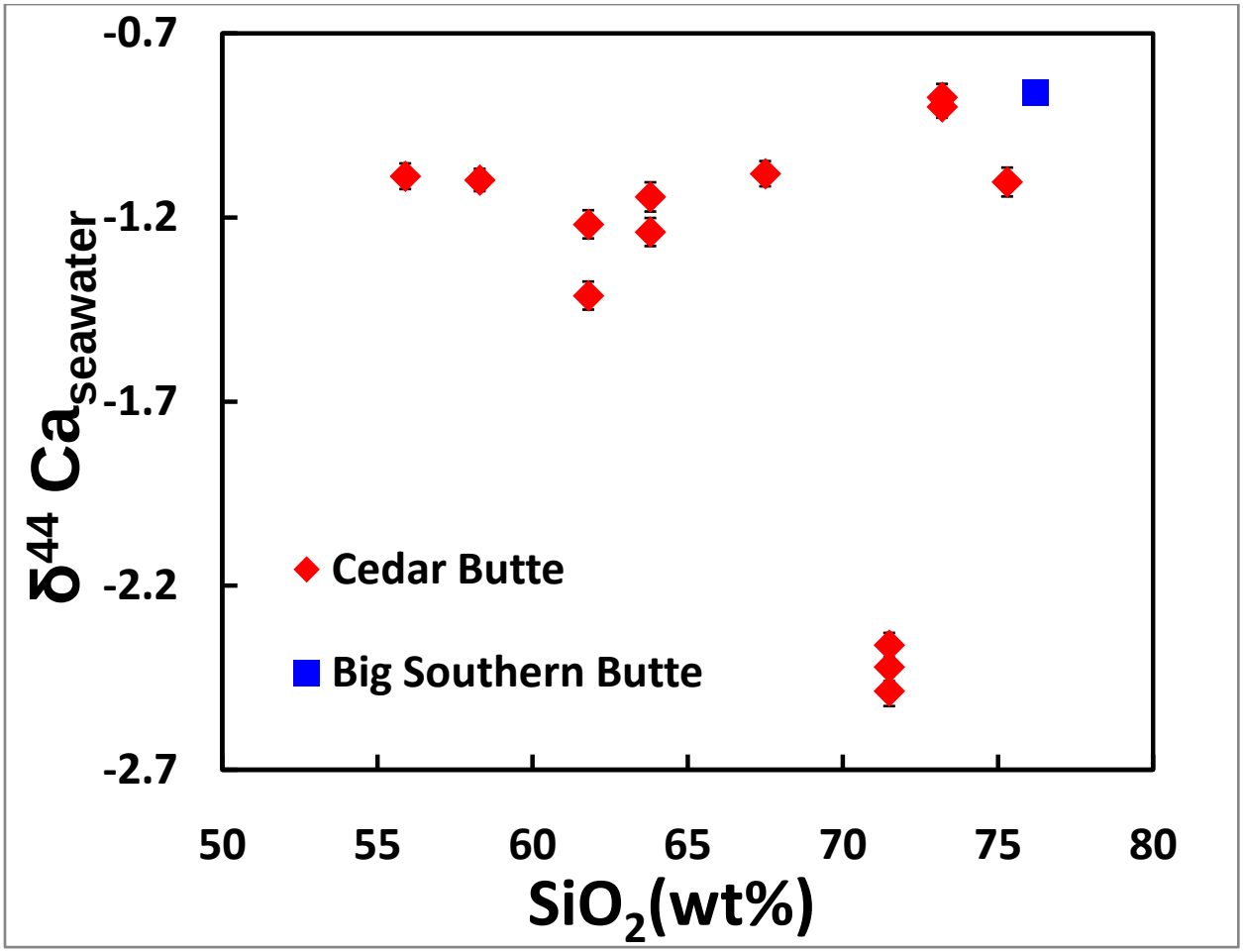

Fig. 4a. Calcium isotope composition of Cedar Butte rocks as a function of SiO_2 content. Error bars represent 2 times standard error (2SE external reproducibility)

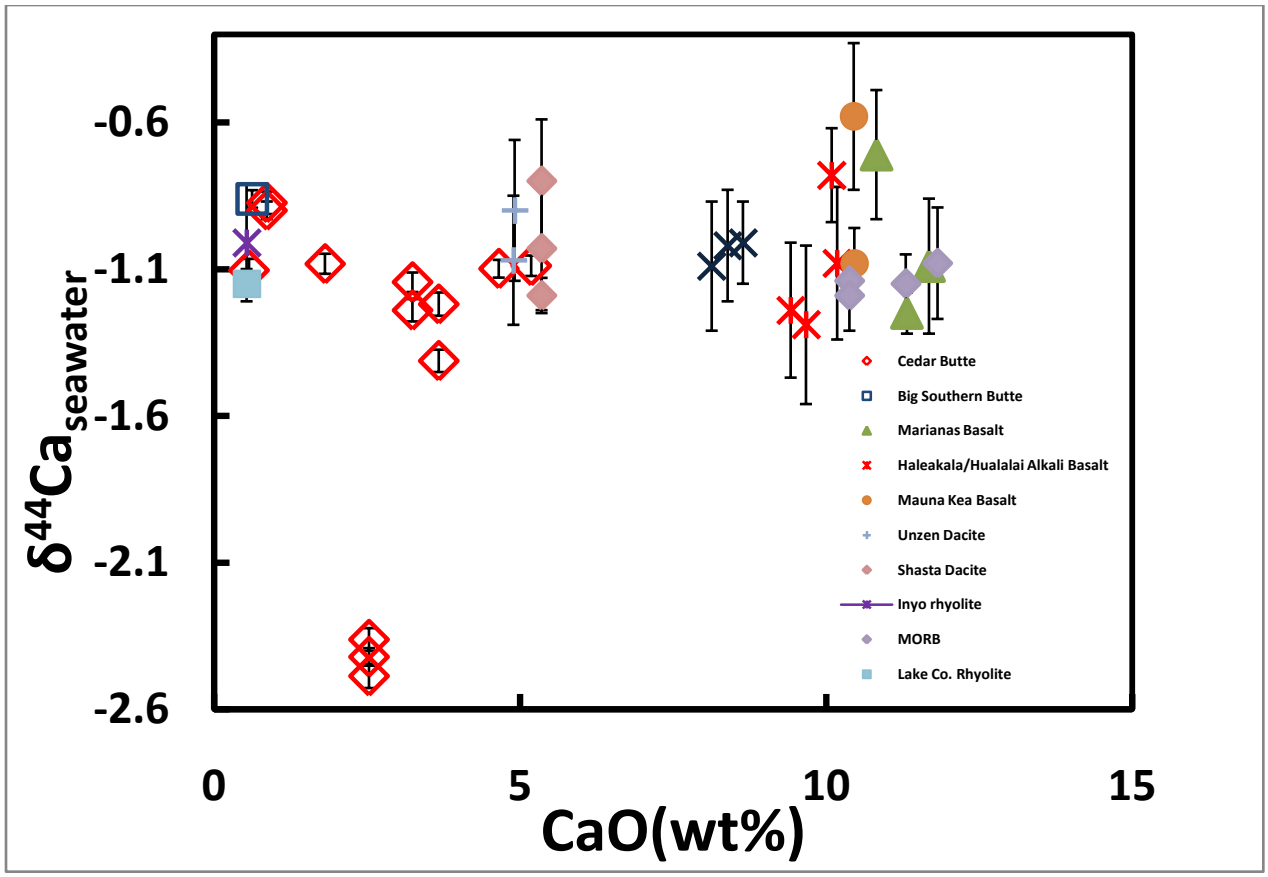

Fig. 4b. Calcium isotope composition of Cedar Butte rocks as a function of CaO content. Previously reported literature $\delta^{44}Ca$ values of terrestrial igneous rocks are shown for comparison (Skulan et al. 1997; DePaolo 1994; Eiler et al. 1996 1997; Sims et al. 1999; Chen et al. 1999; Getty and DePaolo 1995; Richter et al. 2003).

CHAPTER 5

Discussion

1. Mechanisms of production of rhyolite

Conventionally people think that the chemical diversity of igneous rocks, most readily manifested as the variation in silica content, is the result of partial melting and fractional crystallization of magma. Assimilation by partial melting of the crust, coupled to heat produced by fractional crystallization (AFC), is the most often invoked mechanism to produce high silica content magmas in the crust.

My results for both Fe and Ca show significant isotopic fractionation occurring within the Cedar Butte differentiation sequence. For the δ^{56}Fe results, there is a clear relationship between δ^{56}Fe and extent of differentiation. The origin of these isotopic variations remains highly debated but the clear tie to differentiation brings added significance to the question of how the isotopes fractionate because they may help distinguish the differentiation process. Here I assess various proposed explanations for these variations including crustal assimilation and/or fractional crystallization (Schuessler et al., 2008), loss of a hydrous fluid (e.g. Heimann et al) and/or temperature gradient based differentiation (e.g. Lundstrom, 2009).

1.1 Partial melting of the crust

Previously, Leeman, (1982b) proposed a model in which the rhyolites along the Yellowstone hotspot track formed by the partial melting of the crust. The Nd and Sr isotopic features of ESRP rhyolites (ε_{Nd} = -4~-6; $^{87}Sr_i/^{86}Sr_i$ =~0.708 to 0.7097) though, are strongly distinctive from those of the highly evolved Archean crustal rocks (ε_{Nd} = -23~-47; $^{87}Sr_i/^{86}Sr_i$ =0.702~0.892) (Leeman et al., 1985), which precludes the possibility that ESRP volcanic

rhyolites formed solely by melting of Archean crust. A modified model that produced silicic melts by hybridization of basalts with preexisting crust as proposed by Hildreth, (1991), has been called upon to generate more mantle-like isotopic signatures. However, based on a simple mixing calculation with combinations of olivine tholeiite (Hughes et al., 2002) and Archean crust (Leeman et al., 1985), crustal materials could only contribute less than 10% mass to Cedar Butte volcanic rocks (McCurry et al. 2008).

1.2 Fractional crystallization

Based on the models presented by Leeman et al. (1976) and Thompson (1975), Spear (1979) first proposed that trachyte at Cedar Butte reflects fractional crystallization of basaltic trachyandesite. McCurry et al., (2008) use an energy-constrained model (EC-AFC) (Spera and Bohrson, 2001; Bohrson and Spera, 2001) to evaluate the combination of assimilation and fractional crystallization, finding that the model is consistent with observed compositional and mineralogical features of ESRP volcanic rocks. In general, the features of Cedar Butte rocks can be explained as reflecting the dominating contributions of fractional crystallization of a basaltic trachyandesite parent magma as well as slight magma mixing with silicic melt from crust to form the silicic magmas (McCurry et al. 2008).

Magnetite is the phase appearing to most control Fe evolution at Cedar Butte (McCurry et al. 2008). Shahar et al. (2008) measured the magnetite-fayalite equilibrium fractionation factor allowing reasonably good constraint on estimating the overall magnetite-bulk melt fractionation factor. By treating fractional crystallization as a Rayleigh process, we can apply the fractionation factor to estimate Fe isotope fractionation in this process. In this model, sample CB-91-7, as the least evolved rock, was chosen to represent the source of the rock series and a fractionation factor $\Delta^{56}Fe_{mag\text{-}fa}$ =0.16 between magnetite and melt was used based on the equation $10^3 \ln \alpha^{57}_{mag\text{-}}$

$_{fa}=\Delta^{57}Fe_{mag\text{-}fa}=0.30\ (\pm 0.24)\times 10^6/T^2$ (A. Shahar et al., 2008), assuming the temperature is 850 °C. This simplistic model would predict that evolved magmas would become isotopically lighter during fractional crystallization if magnetite were the major fractionation phase controlling Fe content of the magma (A. Shahar et al., 2008); this is opposite to observed Cedar Butte isotopic features (Fig. 5). Unpublished results for Mgt-melt-fluid from the UIUC laboratory give the same sense of fractionation with magnetite isotopically heavier than coexisting melt. Thus both the Shahar et al. (2008) data and the UIUC data agree with theory that the concentration of Fe^{+3} into magnetite should lead to magnetite being isotopically heavy (Polykov and Mineev, 2000). Thus, the Fe isotopic changes during magmatic differentiation at Cedar Butte appear to be inconsistent with fractional crystallization or AFC.

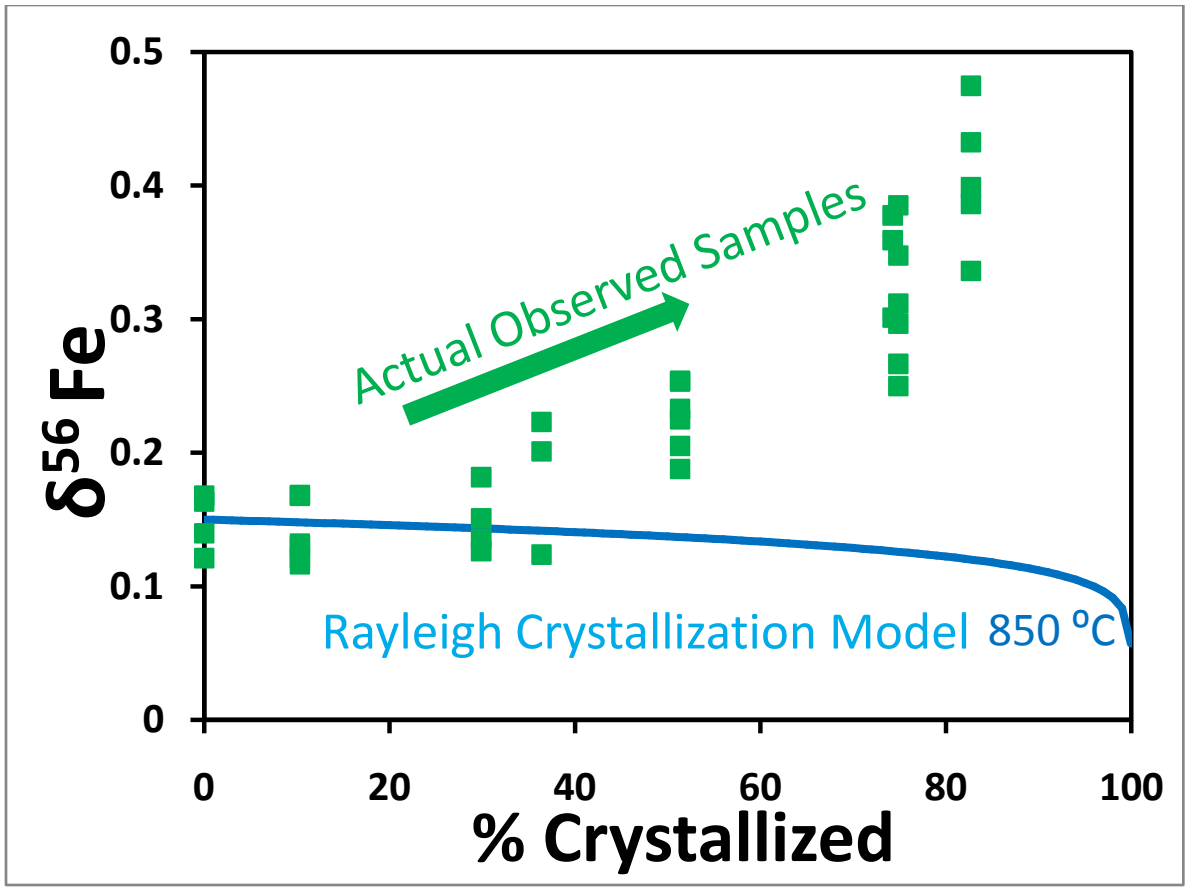

Fig. 5. Rayleigh fractionation model for Fe isotope fractionation during differentiation of an andesitic parent magma by fractional crystallization including magnetite at 850 °C, using the fractionation factor between magnetite and fayalite by A. Shahar et al., (2008). This Model predicts that δ^{56}Fe should be lighter in the more differentiated samples, which is opposite to observed.

1.3 Loss of a Hydrous Fluid

Poitrasson and Freydier, 2005 proposed a hypothesis that the preferential removal of light iron from the magmas by aqueous fluids exsolved during late evolution stage is responsible for the heavier Fe isotope composition of highly differentiated igneous rocks. The sharp drop in H_2O solubility with silica content increasing beyond 71 wt. % SiO_2 (Wyllie, 1977) can lead to aqueous fluid exsolution which may results in Fe oxidation of highly differentiated, Fe-poor melts (Candela, 1986) and reducing exsolved fluids (Rowins et al., 1991). These reduced deuteric fluids would therefore be enriched in isotopically light Fe^{2+} and then can cause an enrichment in heavy Fe isotopes of the residual melt (Poitrasson and Freydier, 2005).

The partition coefficients and isotope fractionation factors for Fe between fluids and melts are poorly constrained and a realistic quantitative model is not available yet. However, a simplified Rayleigh distillation model can be used to estimate the influence of fluid-magma interaction on Fe isotopes by assuming that the Fe isotope fractionation is completely controlled by the removal of fluid from solid. An estimated upper limit of $\Delta^{56}Fe_{fluid\text{-}solid}$= -0.5‰ at magmatic temperatures is used in this model. The fluid exsolution occurs in highly differentiated magmas, thus this model focuses only on the high silica part of the suite; sample CB-91-13 (SiO_2 = 67.5 wt. %, FeO* = 6.8 wt. %,) was chosen to be the starting material. The model predicts that the $\delta^{56}Fe$ values of bulk rocks will become progressively heavier as temperature decreases and Fe chloride-bearing fluid exsolves (Fig. 6), which is in agreement with observed Cedar Butte values. The size of the fractionation factor 0.5 per mil, is probably high by an order of magnitude.

The solubility experiments of Chou and Eugster (1977) suggest that 0.24- 16.4 wt. % at 700-500 ℃ of Fe (as $FeCl_2$ species) can be present in a chloride- rich fluid (up to 40 wt. % $NaCl_{eq}$). A Exsolution of about up to 5 wt. % H_2O dissolved in the silicate melt may typical for siliceous

magmas. Compared to these realistic constraints, the model parameters used in the Rayleigh calculation overestimate the real conditions at Cedar Butte to a great extent and much smaller fractionation are more likely to occur in nature. Hence the increase in $\delta^{56}Fe$ values of Cedar Butte samples from intermediate rocks to rhyolites does not likely result from exsolution of Fe^{2+}-bearing fluids alone.

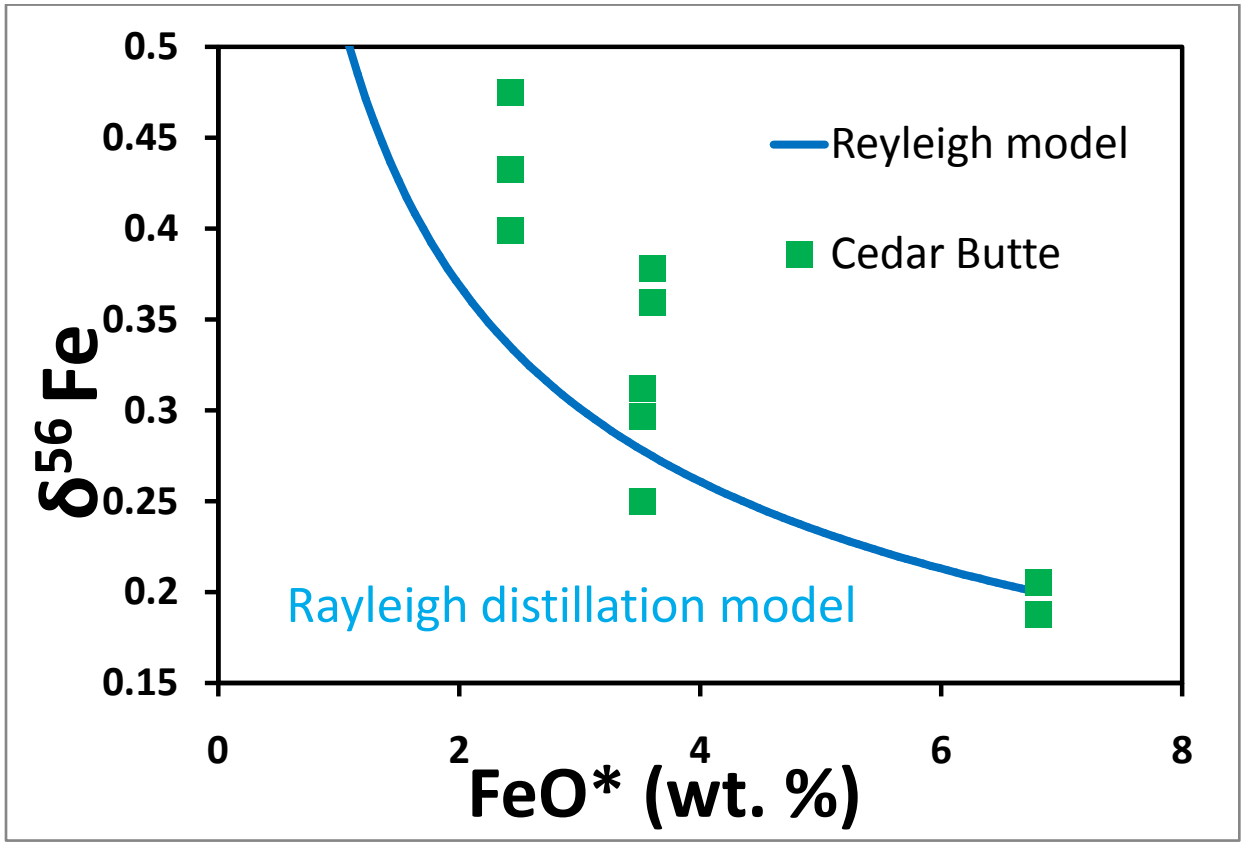

Fig. 6. Rayleigh fractionation model for Fe isotope fractionation during removal of low- $\delta^{56}Fe$ fluid through volatile loss, using an estimated fractionation factor of -0.5 between fluid and bulk solid. This model predicts that $\delta^{56}Fe$ should be heavier in the more differentiated samples, which is consistent with observed.

2. Thermal diffusion

There are two kinds of processes taking place in a thermal gradient: a Soret process if it occurs in a single liquid phase and a thermal migration process if it occurs in partially molten material (Huang et al., 2009). Both processes involve chemical diffusion (driven by a chemical activity gradient) and thermal diffusion (driven by a temperature gradient).

The effects of temperature gradients on magma composition have been considered since Bowen (1921, 1928). He argued that the rate of heat conduction is orders of magnitude faster than mass diffusion such that temperature contrasts will be spatially dissipated by conduction in a short time before mass can diffuse. Hence the thermal gradient driven diffusion will be impeded from accomplishing much fractionation (Walker and DeLong, 1982). Another argument Bowen (1928) proposed is that the magnitude of this effect was expected to be small which has been proved false by many experiments below.

However, the heat conduction argument was based on the simple idea that magma bodies reflected injection of a single blob of magma followed by cooling. This has been questioned by recent studies suggesting incremental emplacement. The lifetime of a temperature gradient can be prolonged by thermal input from below, which provides the temporal precondition for thermal driven diffusion to essentially take effect.

2.1 A thermal diffusion model for magmas formation

The existence of vertical thermal zoning for an igneous magma body has been shown by many studies (e.g. Lipman, 1971; Hildreth, 1979). There is plenty of experimental work examining the compositional changes driven by temperature gradients through silicate materials done in the 1980's. Previous works have confirmed that chemical differentiation can be induced by a thermal gradient (Walker et al., 1981, 1988; Walker and DeLong, 1982; Lesher and Walker, 1986, 1988).

It is demonstrated that a granitic bulk composition will accumulate at the cold end while a more mafic composition forms at the hot end when an originally homogeneous wet andesite is placed in a thermal gradient under partially molten conditions (Huang et al. 2009). The major- and trace- element patterns produced by thermal migration reflect the systematic change in modal mineralogy. They are consistent with the differentiation trends produced by fractional crystallization meaning that the observed compositional characteristics in silicic rock suites including Cedar Butte volcanic rocks could be explained by this process (Huang et al., 2009).

Lundstrom (2009) proposed a model called thermal migration zone refining (TMZR) to explain the formation of granitoids. It is also a possible mechanism for forming the zoned magma chamber beneath Cedar Butte prior to eruption. In this model, there are continuous injections of trachy-andesitic magmas from below and this maintains a near steady-state, vertical temperature gradient. The thermal migration zone refining process is initiated when magmas are halted by a permeability or density barrier and begin to underplate, which leads to wet thermal migration occurring in the material overlying the most recent sill of injection. As the heat source moves down with time, the thermal gradient zone moves downward at the underplating rate; a compositionally zoned mush is formed after several injections and cooling cycles with the rhyolite accumulated on top at the cold end and basaltic trachyandesite below at the hot end.

Finally an event of magma injection leads to wholesale melting of the mush and triggers the eruption of the felsic to mafic lava sequence that is consistent with the eruptive sequence of Cedar Butte volcanic rock suite. The fact that this process is one of low melt volume and incremental assembly successfully solves the long argued geophysical evidence for lack of magma blobs and the space problems mentioned above. This work does not deal with the physical process involved in the eruption but instead simply assumes that this can happen.

3. Isotopic fractionations through thermal diffusion

It is only recently that it has been realized that isotopes could be fractionated by a thermal gradient in silicate melts. Experimental work on oxygen showed extraordinarily large isotopic fractionations in Soret experiments (Kyser et al., 1998). Significant iron, calcium and magnesium isotopic signatures were found more recently (Huang et al., 2010; Richter et al., 2008). Significant iron and magnesium isotopic fractionations can also be found in thermal migration experiments (~ 2.8‰ for δ^{56}Fe and ~9.9‰ for δ^{26}Mg for the melt bearing portion of the experiments) (Huang et al., 2009).

The experiments show that considerable fractionation occurs during thermal diffusion for several stable isotopes and suggest that the same signatures could occur in natural rocks (Lundstrom, 2009). The observation that the lighter isotopes are enriched at the hot end and the heavier isotopes at the cold end for all isotopic systems make predictions quite simple (Kyser et al., 1998; Richter et al., 2008). Despite the complicated natural system in which isotopic exchange would be buffered and thus inefficient, significant isotopic fractionation should still be observable (Lundstrom, 2009). While isotopic fractionation /℃ of the size observed in experiments is unlikely (because of inefficient exchange), one straightforward prediction is positive o-variation between different isotope systems. Indeed, Lacks et al (2012) show that the isotopic fractionation does not depend on the magnitude of the thermal gradient but simply scales with offset in temperatures. This predicts that if thermal migration plays a critical role in the development of magmas, heavy isotopic compositions will accumulated in the cold overlying silicic rocks and a lighter isotopic composition will occur in hotter underlying mafic rocks.

3.1 Fe isotope fractionations through thermal diffusion

The δ^{56}Fe of Cedar Butte samples exhibits a systematic light to heavy trend with increasing SiO_2 content (~0.15‰ to 0.45‰) and inferred stratigraphic position in the chamber (Figure 2a). The variation is especially obvious at high SiO_2 range (>65%) where samples becomes FeO poor. Qualitatively, exchange between melt (where isotopic fractionation occurs) and a rock with lower FeO (the most differentiated CB samples) will be more effective. Since silica is also inferred to increase stratigraphically upward in the magma chamber, both composition and isotopic change is consistent with the prediction of TMZR model.

3.2 Ca isotope fractionations through thermal diffusion

Unlike iron, calcium has only one oxidation state (+2) and no fractionations are associated with redox conditions. Equilibrium fractionation occurs as a consequence of covalent atomic bonding and Ca tends to form ionic rather than covalent bonds in minerals (O'Neil, 1986) Hence the Ca isotopic variations observed in nature are mostly attributed to kinetic effects (DePaolo, 2006). Many experiments have confirmed that diffusion within silicate melts can fractionate Ca isotopes significantly (e.g. chemical diffusion by Richter et al. 2003). Huang et al. (2010) investigated the isotope fractionations through thermal diffusion in silicate melts and discovered an enrichment of heavy Ca isotopes at the cold end. While the δ^{44}Ca of Cedar Butte samples are not as straightforward as the Fe data, they also exhibit a roughly systematic light to heavy trend with increasing SiO_2 content (Figure 4a), which agrees with the thermal diffusion experimental results.

The discovery that isotopic fractionation of iron, calcium and magnesium is independent of melt composition and that the isotope ratios display a positive covariation with each other provides the fingerprint to identify the existence of thermal migration processes (Huang et al.

2010). The positive co-variation trend between $\delta^{44}Ca$ and $\delta^{56}Fe$ values for Cedar Butte samples shown in Fig. 7 is consistent with the experimental prediction and gives solid evidence for a role for thermal diffusion in the origin of the compositionally zoned magma chamber of Cedar Butte.

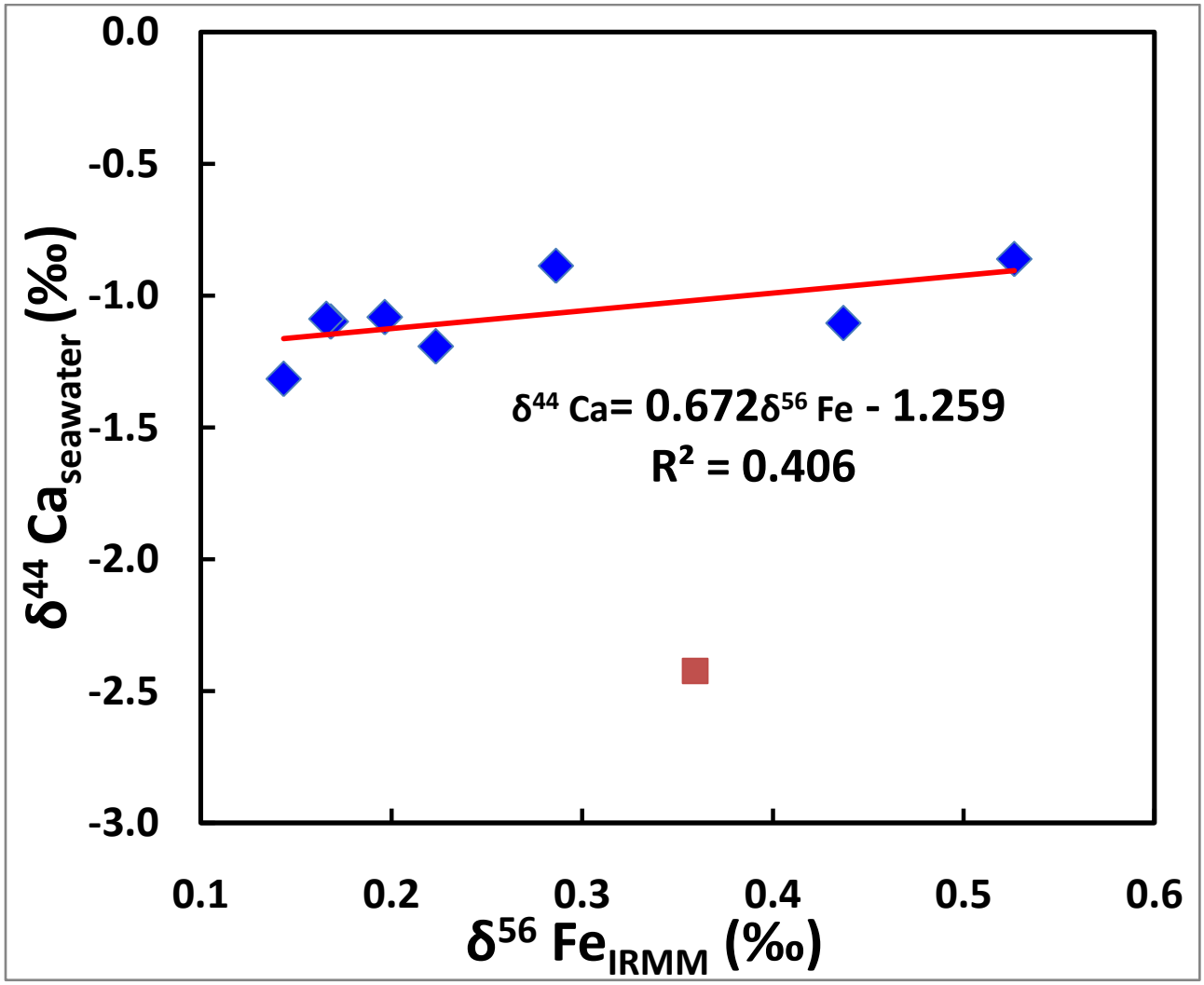

Fig. 7. Positive covariant trend between $\delta^{44}Ca$ and $\delta^{56}Fe$ values for Cedar Butte samples.

CHAPTER 6

CONCLUSIONS

The behavior of Fe and Ca isotopes during magma differentiation was investigated on eruption products from Cedar Butte volcano. The results show an enrichment of heavy isotopes in evolved rhyolitic rock samples; no systematic variations in $\delta^{56}Fe$ and $\delta^{44}Ca$ were found in the more mafic basaltic trachyandesite to trachydacite samples. Generally the isotope compositions of the samples arepositively correlated with indicators of magma differentiation, suggesting that thermal migration, rather than fractionation crystallization, plays the most important role in the magma differentiation process of Cedar Butte.

References:

Albarede F, Beard B. (2004) Analytical methods for non-traditional isotopes. Geochemistry of Non-traditional stable isotopes. Reviews in mineralogy and geochemistry. pp 113-152.

Annen C., Scaillet B. and Sparks R. S. J. (2006) Thermal constraints on the emplacement rate of a large intrusive complex; the Manaslu Leucogranite, Nepal Himalaya. *J. Petrol.* **47,** 71-95.

Bachmann O, Bergantz GW (2004) On the origin of crystal-poor rhyolites: extracted from batholithic crystal mushes. J Petrol 45:1565–1582.

Beard, B.L., Johnson, C.M., Skulan, J.L., Nealson, K.H.,Cox, L., Sun, H., 2003. Application of Fe isotopes to tracing the geochemical and biological cycling of Fe. Chem. Geol. 195, 87–117.

Bowen, N. L. (1921). Diffusion in silicate melts. J Geol 29: 295-317.

Bowen, N. L. (1928). The Evolution of Igneous Rocks. New York: Dover, 332 pp.

Bohrson WA, Spera FJ (2001) Energy-constrained open-system magmatic processes II: general model and energy-constrained assimilation and fractional crystallization (EC-AFC) formulation. J Petrol 42:1019 – 1041.

Bonnichsen B, Leeman WP, Honjo N, McIntosh WC, Godchaux MM (2007) Miocene silicic volcanism in southwestern Idaho: geochronology, geochemistry, and evolution of the central Snake River Plain. Bull Volcanol 70:361-383.

Boroughs S, Wolff J, Bonnichsen B, Godchaux M, Larson P (2005) Large volume, low-^{18}O rhyolites of the central Snake River Plain, Idaho, USA. Geology 33:821–824.

Brian L. Beard and Clark M. Johnson (2004) Fe Isotope Variations in the Modern and Ancient Earth and Other Planetary Bodies. *in* Johnson C. M., Beard B. L., Albarede F., Geochemistry of Non-traditional stable Isotopes. Reviews in Mineralogy & Geochemistry Volume 55, pp319-357

Butler IB, Archer C, Vance D, Oldroyd A, Rickard D. (2005). Fe isotope fractionation on FeS formation in ambient aqueous solution. Earth Planet Sci Lett 236:430-442.

Candela PA, (1986) The evolution of aqueous vapor from silicate melts: effect on oxygen figacity. Geochim. Cosmochim. Acta 50, 1205-1211

Chen, C. F. & Turner, J. S. (1980) Crystallization in double-diffusive system. Journal of Geophysical Research 85, 2573–2593.

Chen CH, Nakada S, Shieh YN, DePaolo DJ (1999) The Sr, Nd and O isotopic studies of the 1991-1995 eruption at Unzen. Japan J volc Geothermal Res 89: 243-253 (1999)

Chou IM. and Eugster HP (1977) Solubility of magnetite in supercritical chloride solutions. Am. J. Sci. 277, 1296-1314

Christiansen E, McCurry M (2008) Contrasting origins of Cenozoic silicic volcanic rocks from the western Cordillera of the United States. Bull Volcanol 70: 417-434.

Clemens J.D., AND Mawer C.K., 1992, Granitic magma transport by fracture propagation: Tectonophysics, v. 204, p. 339-360.

Coleman D, Gray W, Glazner A. F (2004) Rethinking the emplacement and evolution of zoned plutons: Geochronologic evidence for incremental assembly of the Tuolumne Intrusive Suite, California. Geology 32: 4 433-436.

Dauphas N and Rouxel O. (2006) Mass spectrometry and natural variations of iron isotopes. Mass spectrometry reviews 25, 515-550.

Dauphas N., Pourmand A and Teng F-Z. (2009). Routine isotopic analysis of iron by HR-MC-ICPMS: How precise and how accurate? Chemical Geology 267, 175-184.

Dauphas, N., van Zuilen, M., Wadhwa, M., Davis, A.M., Marty, B., Janney, P.E., 2004. Clues from Fe isotope variations on the origin of Early Archean BIFs from Greenland. Science 306, 2077–2080.

DePaolo D. J. (2004) Calcium Isotopic Variations Produced by Biological, Kinetic, Radiogenic and Nucleosynthetic Processes. *in* Johnson C. M., Beard B. L., Albarede F., Geochemistry of Non-traditional stable Isotopes. Reviews in Mineralogy & Geochemistry Volume 55, pp255-288

Getty SJ, DePaolo DJ (1995) Quaternary geochrononology by the U-Th-Pb method. Geochim Cosmochim Acta 59: 3267-3272

Glazner A. F., Bartley J. M., Coleman D. S., Gray W., and Taylor R. Z. (2004) Are plutons assembled over millions of years by amalgamtion from samll magma chambers? *GSA Today* **14**, 4-7.

Green, J. C. & Fitz-Thomas, J. I. (1993). Extensive felsic lavas and rheoignimbrites in the Keweenawan Midcontinent Rift plateau volcanics, Minnesota; petrographic and field recognition. Journal of Volcanology and Geothermal Research 54, 177–196.

Eiler JM, Valley JW, Stolper EM (1996) Oxygen isotope ratios in olivine from the Hawaii Scientific Drilling Project. J Geophys Res-Solid Earth. 101(B5): 11807-11813

Eiler JM, Farley KA, Valley JW, Hauri E, Craig H, Hart SR, Stolper EM (1997) Oxygen isotope variations in ocean island basalt phenocrysts. Geochim Cosmochim Acta 61: 2281-2293

Lundstrom C. (2009) Hypothesis for the origin of convergent margin granitoids and Earth's continental crust by thermal migration zone refining. Geochimica et Cosmochimica Acta 73 5709-5729.

Hayden K P., (1992) The Geology and Petrology of Cedar Butte, Bingham County, Idaho. Master thesis in Geology, Idaho State University.

Hildreth W. (1979) The Bishop Tuff: evidence for the origin of compositional zonation in siticic magma chambers. *Geol. Soc. Am. Spec. Pap.* **180**, 43-75.

Hildreth, W., Halliday, A. N. & Christiansen, R. L. (1991). Isotopic and chemical evidence

concerning the genesis and contamination of basaltic and rhyolitic magma beneath the Yellowstone Plateau volcanic field. Journal of Petrology 32, 63–137.

Holmden C. and Belanger N. (2010) Ca isotope cycling in a forested ecosystem Geochim. Cosmochim. Acta 74, 995-1015.

Holmden C., Papanastassiou D A., Blanchon P., Evans S. (2012) $\delta^{44/40}$Ca variability in shallow water carbonates and the impact of submarine groundwater discharge on Ca-cycling in maring environments. Geochimica et Cosmochimica Acta 83 179-194

Huang F et al. (2009) Thermal Migration in Wet Andesite: Experiments and models suggesting a new mechanism of magma differentiation. *Geochimica et Cosmochimica Acta.*73 729-749.

Hughes SS, McCurry M, Geist DJ (2002) Geochemical correlations and implications for the magmatic evolution of basalt flow groups at the Idaho National Engineering and Environmental Laboratory. In: Mink LL, Link PK (eds) Geology, hydrogeology, and environmental remediation: Idaho National Engineering and Environmental Laboratory, Eastern Snake River Plain, Idaho. Geol Soc Am Spec Pap 353:151 – 173.

Kistler R. and Fleck R. (1994) Field guide for a transect of the central Sierra Nevada, California; geochronology and isotope geology. *Open-File Report - U. S. Geological Survey, Report: OF 94-0267, 50 pp.*

Kuntz M.A., Dalrymple B.G., Champion D.E., Doherty D.J. (1980) Petrology, age, paleomagnetism of volcanic rocks at the Radioactive waste management Complex, Idaho National Engineering Laboratory, Idaho, with an evaluation of potential volcanic hazards: United States Department of the Interior Geological Survey Open File Report 80-388

Kuntz M.A., Champion D.E., Spiker E.C., Lefebvre R.H. (1986) Contrasting magma types and steady-state, volume- predictable volcanism along the Great Rift, Idaho. Geol Soc Amer Bull 97: 579-594.

Kyser T. K., Lesher C. E., and Walker D. (1998) The effects of liquid immiscibility and thermal diffusion on oxygen isotopes in silicate liquids. *Contributions to Mineralogy and Petrology* **133**, 373-381.

Leeman WP (1982a) Olivine tholeiite basalts of the Snake River Plain, Idaho. In: Bonnichsen B, Breckenridge RM (eds) Cenozoic geology of Idaho. Idaho Bur Mines Geol Bull 26:181-191.

Leeman WP (1982b) Rhyolites of the Snake River Plain – Yellowstone Plateau province, Idaho and Wyoming: A summary of petrogenetic models. In: Bonnichsen B, Breckenridge RM (eds) Cenozoic geology of Idaho. Idaho Bur Mines Geol Bull 26:203 – 212.

Leeman WP, Vitaliano CJ, Prinz M (1976) Evolved lavas from the Snake River Plain, Craters of the Moon National Monument, Idaho. Contrib Mineral Petrol 56:35–60.

Leeman WP, Menzies MA, Matty DJ, Embree GF (1985) Strontium, neodymium and lead isotopic compositions of deep crustal xenoliths from the Snake River Plain: evidence for Archean basement. Earth Planet Sci Lett 75:354 – 468.

Lesher C. E. and Walker D. (1986) Solution properties of silicate liquids from thermal diffusion experiments. *Geochimica et Cosmochimica Acta* **50**, 1397-1411.

Lesher C. E. and Walker D. (1988) Cumulate Maturation and Melt Migration in a Temperature gradient. *Journal of Geophysical Research* **B9**, 10295-10311.

Lindsay, J. M., Schmitt, A. K., Trumbull, R. B., De Silva, S. L., Siebel, W. & Emmermann, R. (2001). Magmatic evolution of the La Pacana caldera system, Central Andes, Chile: compositional variation of two cogenetic, large-volume felsic ignimbrites. Journal of Petrology 42, 459–486.

Lipman P. W. (1971) Iron-titanium oxide phenocrysts in compositionally zoned ash-flow sheets from southern Nevada. *J. Geol.* **79,** 438-456.

Mabey D. R. (1982) Geophysics and tectonics of the Snake River Plain, Idaho. Cenozoic

Geology of Idaho: Idaho Bureau of Mines and Geology Bulletin 26, p. 139-153

Marsh, B. D. (1981). On the crystallinity, probability of occurrence, and rheology of lava and magma. Contributions to Mineralogy and Petrology 78, 85–98.

McBirney, A. R. (1980). Mixing and unmixing of magmas. Journal of Volcanology and Geothermal Research 7, 357–371.

McCurry M, Hayden K, Morse L (2008) Genesis of post-hotspot A type rhyolite of the Eastern River Plain volcanic province by extreme fractional crystallization of olivine tholeiite basalt. *Bull Volcanol* 70:361-383.

Michael, P. J. (1983). Chemical differentiation of the Bishop Tuff and other high-silica magmas through crystallization processes. Geology 11, 31–34.

Nekvasil H, Simon A, Lindsley DH (2000) Crystal fractionation and the evolution of intra-plate hy-normative igneous suites: insights from their feldspars. J Petrol 41:1743–1757.

O'Neil J. R. (1986) Theoretical and experimental aspects of isotopic fractionation. In Valley JW, O'Neil JR and Taylor HR, Stable Isotopes in High Temperature Geological Prosses. Reviews of Mineralogy. pp 561-570.

Paterson S. R. and Vernon R. H. (1995) Bursting the bubble of ballooning plutons; a return to nested diapirs emplaced by multiple processes. Geological Society of America Bulletin 107, 1356-1380.

Pierce K.L, Morgan L.A. (1992) The track of the Yellowstone hot spot: Volcanism, faulting, and uplift. In: Link PK, Kuntz MA, Platt L(eds) Regional geology of eastern Idaho and western Wyoming. Geological Society of America Memoir 179:1–53

Poitrasson F. and Freydier R. (2005) Heavy iron isotope composition of granites determined by high resolution MC-ICP-MS. *Chemical Geology* **222**, 132-147.

Poitrasson, F., Halliday, A.N., Lee, D.C., Levasseur, S., Teutsch, N., (2004). Iron isotope

differences between Earth, Moon, Mars and Vesta as possible records of contrasted accretion mechanisms. Earth Planet. Sci. Lett. 223, 253–266.

Polyakov VB, Mineev SD, (2000). The use of Mossbauer spectroscopy in stable isotope geochemistry. Geochim Cosmochim Acta 61: 4213-4217

Ressell W. A., Papanastassiou D. A., Tombrello T. A. (1978) Ca isotope fractionation on the Earth and other solar sysem materials. Geochim Cosmochim Acta 42: 1075-1090

Riley, T. R., Leat, P. T., Pankhurst, R. J. & Harris, C. (2001). Origins of large volume rhyolitic volcanism in the Antarctic Peninsula and Patagonia by crustal melting. Journal of Petrology 42, 1043–1065.

Richter FM, Davis AM, DePaolo DJ, Watson EB (2003) Isotope fractionation by chemical diffusion between molten basalt and rhyolite. Geochim Cosmochim Acta 67: 3905-3923

Richter F. M., Watson E. B., Mendybaev R., Teng F.-Z., and Janney P. (2008) Magnesium Isotope Fractionation in Silicate Melts by Chemical and Thermal Diffusion. *Geochimica et Cosmochimica Acta* **72**, 206-220.

Rodgers D.W., Hackett W.R., and Ore T. H., (1990) Extension of the Yellowstone Plateau, eastern Snake River Plain, and Owyhee plateau: Geology, V. 18, P. 1138-1141

Rouxel O, Dobbek N, Ludden J, Fouquet Y. (2003). Iron isotope fractionation during oceanic crust alteration. Chem Geol 202: 155-182.

Rowins, SM, Lalonde AE, Cameron EI, (1991). Magmatic oxidation in the syenitic Murdock Creek intrusion, Kirkland Lake, Ontario: evidence from the ferromagnesian silicates. J. Geol. 99,395-414

Rudnick RL (1995) Making continental crust. Nature 378:571–578.

Schuessler J. A., Schoenberg R., Sigmarsson O. (2009) Iron and lithium isotope systematic of the Hekla volcano, Iceland – Evidence for Fe isotope fractionation during magma differentiation.

Chemical Geology 258: 7819.

Schilling F. R. and Partzsch G. M. (2001) Quantifying partial melt fraction in the crust beneath the Central Andes and the Tibetan Plateau. *Physics and Chemistry of the Earth. Part A: Solid Earth and Geodesy* **26**, 239-246.

Schmitt AD, Stille P, Venneman T (2003a) Variations of the $^{44}Ca/^{40}Ca$ ratio in seawater during the past 24 million years: evidence from $\delta^{44}Ca$ and $\delta^{18}O$ values of Miocene phosphate. Geochim Cosmochim Acta 67: 2607-2614

Schmitt AD, Chabaux F, Stille P (2003b) The calcium riverine and hydrothermal isotopic fluxes and the oceanic calcium mass balance. Earth Planet Sci Lett 6731: 1-16

Schoenberg, R., von Blanckenburg, F., (2006) Modes of planetary-scale Fe isotope fractionation. Earth and Planetary Science Letters 252 (3–4), 342–359.

Shahar, A., Young, E.D., Manning, C.E., (2008) Equilibrium high-temperature Fe isotope fractionation between fayalite and magnetite: an experimental calibration. Earth and Planetary Science Letters 268 (3–4), 330–338.

Sims KWW, DePaolo DJ, Murell MT, Baldridge WS, Goldstein S, Clague D, Jull M (1999) Porosity of the melting zone and variations in solid mantle upwelling rate beneath Hawaii: inferences from ^{238}U-^{230}Th-^{226}Ra and ^{235}U-^{231}Pa. Geochim Cosmochim Acta 63: 4119-4138

Skulan J, Depaolo DJ, Owens TL (1997) Biological control of calcium isotopic abundances in the global calcium cycle. Geochim Cosmochim Acta 61: 2505-2510

Smith RB, Braile LW (1994) The Yellowstone hotspot. J Volcanol Geotherm Res 61:121–187

Spear DB (1979) The geology and volcanic history of the Big Southern Butte-East Butte area, eastern Snake River Plain, Idaho. PhD Dissertation, State University of New York Buffalo.

Spera FJ, Bohrson WA (2001) Energy-constrained open-system magmatic processes I: general model and energy-constrained assimilation and fractional crystallization (EC-AFC)

formulation. J Petrol 42:999 – 1018.

Steck, L. K., Thurber, C. H., Fehler, M. C., et al. (1998). Crustal and mantle P wave velocity structure beneath Valles caldera, New Mexico: results from the Jemez teleseismic tomography experiment. Journal of Geophysical Research 103, 24301–24320.

Strelow FEW. (1980). Improved separation of iron from copper and other elements by anion-exchange chromatography on a 4% cross-linked resin with high concentrations of hydrochloric acid. Talanta 27:727–732.

Taylor, P.D.P., Maeck, R., De Bievre, P., (1992). Determination of the absolute isotopic composition and atomic weight of a reference sample of natural iron. Int. J. Mass Spectrom. Ion Processes. 121, 111-125.

Taylor S. R. and White J. R. A. (1965) Geochemistry of andesites and the growth of continents. Nature 208, 271-273.

Taylor, S. R. & McClennan, S. M. (1985). The Continental Crust: its Composition and Evolution. Cambridge, MA: Blackwell, 312 pp.

Thompson RN (1975) Primary basalts and magma genesis; II, Snake River Plain, Idaho, U.S.A. Contrib Mineral Petrol 52:213–232.

Von Blanckenburg F., Fruh-Green G., Diethelm K., and Stille P., (1992) Nd-, Sr-, O-isotopic and 1300 chemical evidence for a two stage contamination history of mantle magma in the Central-1301 Alpine Bergell intrusion, *Contrib. Mineral. Petrol.* **110**, 33-45.

Walker D., Lesher C. E., and Hays J. F. (1981) Soret separation of lunar liquid. *Proc. Lunar Planet. Sci. Conf. 12th.* 991-999.

Walker D. and DeLong S. E. (1982) Soret separation of mid-ocean ridge basalt magma. *Contributions to Mineralogy and Petrology* **79**, 231-240.

Walker D., Jurewicz S., and Watson E. B. (1988a) Adcumulus dunite growth in a laboratory

thermal gradient. *Contrib. Mineral. Petrol.* **99**, 306-319.

Weyer, S. and Schwieters, J.B., (2003). High precision Fe isotope measurements with high mass resolution MC-ICPMS. Int. J. Mass Spectrom. 226, 355-368.

Whitaker ML, Nekvasil H, Lindsley DH, McCurry M (2008) Can crystallization of olivine tholeiite give rise to potassic rhyolites?— An experimental investigation. Bull Volcanol 70: 417-434.

Wyllie PJ, (1977). Crustal anatexis: an experimental review. Tectonophysics 43, 41-71

Table 1. Major(wt%) and trace element (ppm) concentrations in the whole rock samples used

Sample	CB-91-48	CB-91-DI5	CB-91-DI1R	CB-91-21	CB-91-32	CB-91-13	CB-91-4	CB-91-7	BSB-1
SiO_2	61.8	58.3	73.2	75.3	71.5	67.5	63.8	55.9	76.2
TiO_2	0.89	1.55	0.26	0.13	0.24	0.44	0.65	1.77	0.09
Al_2O_3	13.7	13.3	12.9	12.5	12.7	13.8	13.5	13.3	12.6
FeO_{total}	9.8	12.5	3.5	2.4	3.6	6.8	8.9	14.0	1.6
MnO	0.30	0.33	0.09	0.05	0.09	0.15	0.28	0.36	0.04
MgO	0.57	1.27	0.09	0.02	0.25	0.17	0.32	1.53	0
CaO	3.67	4.65	0.86	0.57	2.53	1.81	3.24	5.18	0.62
Na_2O	4.08	3.79	4.10	4.16	4.06	4.01	4.15	3.93	4.27
K_2O	4.90	3.61	4.94	4.91	5.05	5.26	5.00	3.29	4.64
P_2O_5	0.21	0.71	0.05	0.01	0.03	0.05	0.14	0.78	
Total	98.2	97.5	99.8	99.3	97.7	98.1	98.1	98.3	100.1
Ba	2989	2492	702	369	765	1615	2124	2509	
Rb	110	90	225	260	225	156	124	69	
Sr	114	244	18.3	2.6	18	22	64	260	
Sm		28.5	28.8	21.5				29.4	
Nd		139	122	81				146	
Ni	11	6	8	6	9	9	7	6	
Zr	2483	2873	859	468	813	1566	2060	2858	

1. Data are from Michael McCurry and Karl P. Hayden, Department of Geosciences, Idaho State University (Hayden K P., 1992)

Table 2. Iron isotopic compositions of terrestrial volcanic rocks

Sample	SiO_2 (wt. %)	$\delta^{56}Fe$	Uncertainty*	Sample Description	Ref.
EV9101	76.8	0.386	0.027	Peralkaline granite	1
CB9202	77	0.311	0.056	Aluminous hypersolvus granite	1
PC9401	64.9	0.11	0.036	Calc-alkaline granodiorite	1
CA9415	71.3	0.155	0.024	Peraluminous granite	1
SN9402	65.5	0.098	0.03	Calc-alkaline monzogranite	1
PO9207	76.1	0.244	0.025	Aluminous hypersolvus granite	1
9108	77.7	0.232	0.04	Aluminous hypersolvus granite	1
GA	69.9	0.11	0.027	Calc-alkaline granite	1
GSR-1	72.8	0.17	0.04	Biotite granite	1
Siss6	45.92	-0.005	0.046	Central-Alpine Bergell intrusion	2
siss4	46.92	0.04	0.046	Central-Alpine Bergell intrusion	2
siss1	47.95	0.053	0.051	Central-Alpine Bergell intrusion	2
siss2	48.81	0.028	0.051	Central-Alpine Bergell intrusion	2
iorio2	54.89	0.055	0.046	Central-Alpine Bergell intrusion	2
sor1	55.61	0.065	0.075	Central-Alpine Bergell intrusion	2
mer1	56.43	0.061	0.046	Central-Alpine Bergell intrusion	2
ma 1	57.25	0.062	0.052	Central-Alpine Bergell intrusion	2
ge20	57.93	0.071	0.046	Central-Alpine Bergell intrusion	2
iorio1	62.39	0.111	0.046	Central-Alpine Bergell intrusion	2
bona1	66.3	0.097	0.046	Central-Alpine Bergell intrusion	2
bona3	70.67	0.084	0.046	Central-Alpine Bergell intrusion	2
bona2	73.76	0.141	0.052	Central-Alpine Bergell intrusion	2
siss7	75.57	0.226	0.046	Central-Alpine Bergell intrusion	2

1. References: (1)Poitrasson and Freydier, 2005 (2)Schonenberg and von Blanckenberg, 2007
2. *Uncertainty: uncertainties are two times the standard deviation (2SD) for ref. (2) and two times the standard error (2SE) for ref. (1)

Table 3. Fe isotopic composition of standards and Cedar Butte volcanic rocks

Standard/sample	Session	$\delta^{56}Fe$	2SD	$\delta^{57}Fe$	2SD	$\delta^{57}Fe/\delta^{56}Fe$	n	Comments
Standards								
AGV-1	1	0.146	0.173	0.200	0.184	1.370	8	Procedural duplicate
	2	0.150	0.054	0.187	0.172	1.247	8	Run Jan, 2009
	3	0.135	0.185	0.169	0.296	1.257	8	New digestion, Run Feb, 2009
average		0.144	0.144	0.185	0.196	1.291	24	
AGV-1-soln	1	0.118	0.093	0.220	0.171	1.859	7	Long-term storage solution
BCR-1	1	0.090	0.055	0.169	0.086	1.886	8	Run Jan, 2009
	2	0.076	0.152	0.157	0.290	2.060	16	New digestion, Run Feb, 2009
Average		0.083	0.127	0.163	0.239	1.973	24	
BCR-1-soln	1	0.165	0.170	0.241	0.265	1.461	16	Long-term storage solution
	2	0.198	0.173	0.286	0.294	1.443	16	Procedural duplicate
Average		0.182	0.172	0.264	0.279	1.452	32	
BCR-2-soln	1	0.175	0.138	0.270	0.202	1.543	16	Long-term storage solution
Nod-p	1	-0.494	0.050	-0.652	0.108	1.320	8	Run Jan, 2009
	2	-0.454	0.176	-0.646	0.239	1.423	16	New digestion, Run Feb, 2009
Average		-0.474	0.149	-0.650	0.201	1.371	24	
Samples								
CB-91-4	1	0.223	0.182	0.356	0.229	1.594	16	Run Feb, 2009
CB-91-7	1	0.164	0.099	0.248	0.169	1.514	8	Procedural duplicate
	2	0.168	0.132	0.211	0.206	1.258	8	Run Feb, 2009
Average		0.166	0.113	0.229	0.186	1.386	16	
CB-91-13	1	0.188	0.057	0.274	0.140	1.458	8	Run Jan, 2009
	2	0.205	0.087	0.297	0.088	1.448	14	New digestion, Run Feb, 2009
Average		0.196	0.078	0.285	0.109	1.453	22	
CB-91-21	1	0.399	0.068	0.570	0.192	1.429	8	Run Jan, 2009
	2	0.475	0.069	0.718	0.194	1.513	8	New digestion, Run Feb, 2009
Average		0.436	0.103	0.644	0.241	1.471	16	
CB-91-32	1	0.359	0.093	0.552	0.228	1.537	8	Run Feb, 2009
CB-91-48	1	0.151	0.066	0.245	0.059	1.620	8	Run Jan, 2009
	2	0.136	0.179	0.168	0.209	1.237	16	New digestion, Run Feb, 2009
Average		0.143	0.150	0.206	0.184	1.428	24	
CB-91-DI5	1	0.169	0.108	0.224	0.165	1.328	13	Run Jan, 2009
	2	0.168	0.176	0.254	0.307	1.512	16	New digestion, Run Feb, 2009
Average		0.168	0.142	0.239	0.243	1.420	27	
CB-91-DI-1R	1	0.297	0.064	0.459	0.138	1.548	8	Procedural duplicate
	2	0.250	0.165	0.358	0.180	1.431	16	Run Jan, 2009
	3	0.312	0.158	0.525	0.211	1.686	16	New digestion, Run Feb, 2009
Average		0.286	0.151	0.447	0.226	1.555	40	
BSB-1	1	0.529	0.185	0.706	0.171	1.334	16	Run Jan, 2009
	2	0.524	0.124	0.752	0.205	1.437	15	New digestion, Run Feb, 2009
Average		0.526	0.156	0.728	0.328	1.385	31	

1. n represents the number of replicate Fe isotope measurements
2. Uncertainties are two times the standard deviation (2SD) of n replicate measurements

Table 4. Calcium isotopic compositions of Cedar Butte volcanic rocks

Sample	Session	$^{40}Ca/^{44}Ca$	$\delta^{40}Ca$	2SE	2SD	comments
CB-91-21	1	47.144	-1.10	0.04		
CB-91-DI-1R	1	47.134	-0.90	0.03		
	2	47.133	-0.87	0.04		Spike added, new dissolution
average		47.134	-0.89		0.04	
CB-91-32	1	47.209	-2.49	0.04		
	2	47.206	-2.42	0.04		Repeat
	3	47.204	-2.36	0.03		Spike added, new dissolution
average		47.206	-2.42		0.12	
CB-91-13	1	47.143	-1.08	0.03		
CB-91-4	1	47.150	-1.24	0.04		
	2	47.146	-1.14	0.04		Spike added, new dissolution
average		47.148	-1.19		0.13	
CB-91-48	1	47.159	-1.41	0.04		
	2	47.149	-1.22	0.04		Spike added, new dissolution
average		47.154	-1.32		0.27	
CB-91-DI5	1	47.144	-1.10	0.03		
CB-91-7	1	47.143	-1.09	0.03		
BSB-1	1	47.133	-0.86	0.03		Big southern Butte

1. Uncertainties are given as two times the standard error (2SE) of replicate measurements
2. 2SD represents two times the standard deviation of replicate runs

Table 5. Calcium isotopic compositions of terrestrial volcanic rocks

Sample	CaO (wt. %)	$\delta^{40}Ca_{salt}$	2SD	$\delta^{40}Ca_{seawater}$	Sample Description	Ref.
D54G	11.32	-0.33	0.07	-1.25	Basalt, Marianas drege	1
KOO-10	8.13	-0.17	0.22	-1.09	Tholeiitic Basalt, Koolau	1
KOO-21	8.39	-0.10	0.19	-1.02	Tholeiitic Basalt, Koolau	1
KOO-55	8.64	-0.09	0.14	-1.01	Tholeiitic Basalt, Koolau	1
GUG-6	10.82	0.21	0.22	-0.71	Basalt, Marianas	1
ALV-1833	11.68	-0.17	0.23	-1.09	Basalt, Marianas	1
HK-02	10.18	-0.16	0.26	-1.08	Alkali basalt, Haleakala	2
HU-24	9.42	-0.32	0.23	-1.24	Alkali basalt,Hualalai	2
HU-11	9.67	-0.37	0.27	-1.29	Alkali basalt, Haleakala	2
HU-05	10.09	0.14	0.16	-0.78	Alkali basalt,Hualalai	2
HSDP 452	10.46	-0.16	0.12	-1.08	Tholeiitic Basalt, Mauna Kea	1
HSDP 160	10.45	0.34	0.25	-0.58	Alkali basalt, Mauna Kea	1
92-12-29	4.89	-0.15	0.22	-1.07	Unzen Dacite (1992 eruption)	3
94-02-05	4.91	0.02	0.24	-0.9	Unzen Dacite (1994 eruption)	3
76DSH-8	5.35	0.12	0.21	-0.8	Shasta Dacite (Black Butte)	4
76DSH-8	5.35	-0.11	0.21	-1.03	Shasta Dacite, Hornblende	4
76DSH-8	5.35	-0.27	0.06	-1.19	Shasta Dacite, Plagioclase	4
92DLY-113	0.53	-0.09	0.20	-1.01	Inyo rhyolite	
IO-14	11.82	-0.16	0.19	-1.08	Basalt. Indian Ocean MORB	
IO-38	11.30	-0.23	0.10	-1.15	Basalt. Indian Ocean MORB	
SUNY MORB	10.38	-0.22	0.03	-1.14	MORB	5
SUNY MORB	10.38	-0.27	0.12	-1.19	MORB	5
Lake Co. Obsidian	0.53	-0.23	0.05	-1.15	Rhyolite	5

1. Calcium data are from DePaolo 2004, relative to purified salt standard
2. $\delta^{40}Ca_{seawater}$ is the Calcium isotopic value relative to seawater. $\delta^{40}Ca_{seawater} = \delta^{40}Ca_{salt} - 0.92$ (Skulan et al. 1997)
3. Uncertainties are two times the standard deviation 2SD
4. References: (1) Eiler et al. (1996,1997); (2) Sims et al. (1999); (3) Chen et al. (1999); (4) Getty and Depaolo (1995); (5) Richter et al. (2003)